Imaging of the Central Skull Base

Alexandra Borges, MD

KEYWORDS

- Central skull base • CT • MR imaging
- Skull base pathology • Skull base tumors
- Sellar and parasellar lesions

The central skull base (CSB), the ultimate frontier between the intracranial compartment and the extracranial head and neck, can be affected by intrinsic lesions originating from the bony-cartilaginous structures of the skull base proper or by lesions originating from the neighboring structures from the intracranial compartment above or from the extracranial head and neck below. Because clinical assessment of the CSB is limited, cross-sectional imaging has become the mainstay for the diagnosis, treatment planning, and follow-up of patients with skull base lesions.[1–3] Developments in cross-sectional imaging and in surgical and targeted radiation therapy techniques have largely contributed to improve the prognosis of patients with skull base tumors and to decrease the surgical-related morbidity and mortality.[2–6] Multidisciplinary skull base teams, including ear, nose, and throat (ENT) surgeons; neurosurgeons; radiation therapists; radiologists; and oncologists, have been created to provide a comprehensive approach to patients with skull base lesions with the aim of maximizing the chances for long-term survival with the minimum amount of dysfunction and disfigurement possible.[3,6,7]

Cross-sectional imaging can narrow down the differential diagnoses according to the site of origin, pattern of growth, and imaging features of a given lesion; can accurately delineate tumor margins; and can determine the precise relations between the lesion and important surrounding structures.[3,8,9]

This review focuses on the contribution of imaging to patient management, providing a systematic approach to CSB lesions based on an anatomic division of the CSB and on the tissue constituents present in each division. Detailed knowledge of skull base anatomy is required for correct imaging diagnosis and for accurate delineation of lesions.

ANATOMY

Viewed from above, the skull base shows three naturally contoured regions that grossly correspond to the anterior skull base, CSB, and posterior skull base. The CSB makes up the floor of the middle cranial fossa and is mainly composed of the sphenoid and temporal bone anterior to the petrous ridge (**Fig. 1**). It is separated from the anterior skull base by a line that follows the tuberculum sella, the anterior clinoid processes, the posterior margin of the lesser sphenoid wings, and the anterior and superior rim of the greater sphenoid wings and is separated from the posterior skull base by a line following the spheno-occipital synchondrosis medially and the petroclival synchondrosis and superior ridge of the petrous and mastoid bones posteriorly and laterally.[3,4,8–10]

IMAGING APPROACH TO PATHOLOGIC FINDINGS

For diagnostic imaging purposes, it is useful to subdivide the CSB further into midline sagittal, off-midline parasagittal, and lateral compartments by drawing vertical lines passing medially to the petroclival fissure and just lateral to the foramen ovale, respectively (**Fig. 2**).[3,8,9] The midline sagittal compartment includes the body of the sphenoid and the portion of the clivus anterior to the spheno-occipital synchondrosis (basisphenoid),

The reprint of this artical from August 2009 provides readers corrected images for Figures 4E-F, 6A-B, 15C-D, 22A, 25B-F, and 27C-D.

Radiology Departement, Instituto Português de Oncologia de Francisco Gentil- Centro de Lisboa Rua Prof. Lima Basto, 1093, Lisboa, Portugal
E-mail address: borgalexandra@gmail.com

Neuroimag Clin N Am 19 (2009) 669–696
doi:10.1016/j.nic.2009.11.001
1052-5149/09/$ – see front matter

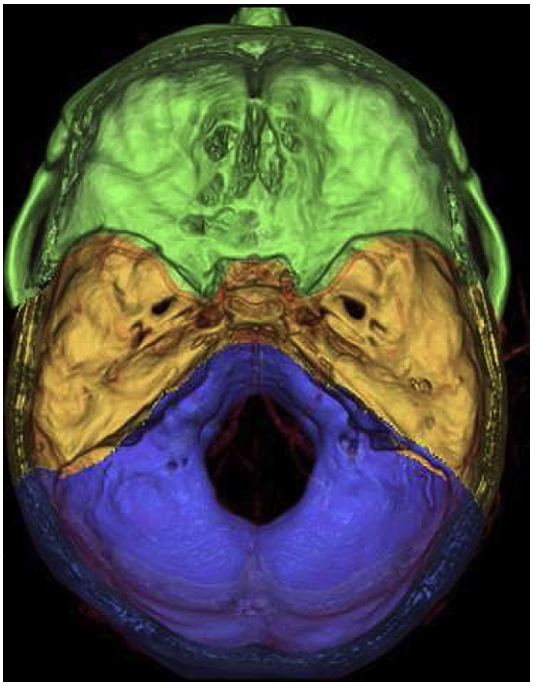

Fig. 1. Three-dimensional CT reconstruction represents the skull base division into anterior (*green*), central (*light orange*), and posterior (*blue*) compartments.

contains the sphenoid sinus, and is bordered superiorly by the sella turcica and inferiorly by the roof and posterior wall of the nasopharynx (**Fig. 3**). It is pierced by the intracranial opening of the orbital apex, giving passage to the optic nerves (**Fig. 4**A). The parasagittal compartment includes the petroclival synchondrosis, foramen

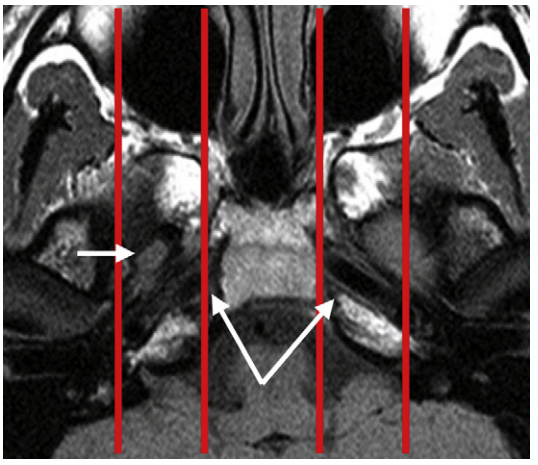

Fig. 2. Axial T1-weighted MR imaging with a schematic representation of the CSB subdivision into sagittal, parasagittal, and lateral compartments. The medial red lines pass in the medial aspect of the petroclival synchondrosis (*long white arrows*). The lateral red lines pass immediately lateral to the foramen ovale (*short white arrow*).

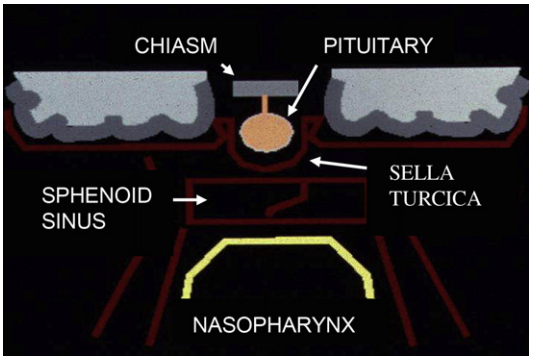

Fig. 3. Schematic representation of the central sagittal skull base with the body of the sphenoid and sphenoid sinus medially, the sella turcica and pituitary gland above, and the nasopharyngeal mucosal space below.

lacerum, and medial aspect of the greater sphenoid wing. It is bordered superiorly and medially by the parasellar region containing the cavernous sinus, superiorly and laterally by the basal temporal lobes, and inferiorly by the parapharyngeal and masticator spaces of the suprahyoid neck. Most of the neurovascular foramina of the CSB lay in this compartment, including the intracranial opening of the superior orbital fissure traversed by cranial nerves III, IV, V1, and VI and the superior ophthalmic vein on their way from the cavernous sinus to the orbit; the foramen rotundum giving passage to V2 on its way from the cavernous sinus to the pterygopalatine fossa; the vidian canal containing the vidian nerve and artery extending from the foramen lacerum to the high pterygopalatine fossa; the foramen ovale traversed by V3 on its way to the masticator space; and the foramen spinosum crossed by the middle meningeal artery. The cavernous sinus, the most important component of the parasagittal CSB, contains, from superior to inferior, cranial nerves III, IV, V1, and V2 enclosed within a dural leaflet of its lateral wall and the cavernous carotid artery and cranial nerve VI within the sinus itself. Finally, the lateral division of the CSB comprises the lateral aspect of the greater sphenoid wing, including the sphenoid triangle, temporal squamosa, and the glenoid cavity of the temporomandibular joint (TMJ).[3,8,9]

In addition to location, knowing the major tissue constituents of the CSB can help in establishing further possible differential diagnoses for a skull base lesion. Although some tissues are common to all subdivisions of the CSB, including bone and the pachymeninges investing the intracranial aspect of the skull base, others are site specific.[8,9] The surgical approach to CSB lesions also varies according to lesion location in each of these compartments (transsphenoidal, transmastoid, temporopteryonal, and frontotemporal approaches).[7,8]

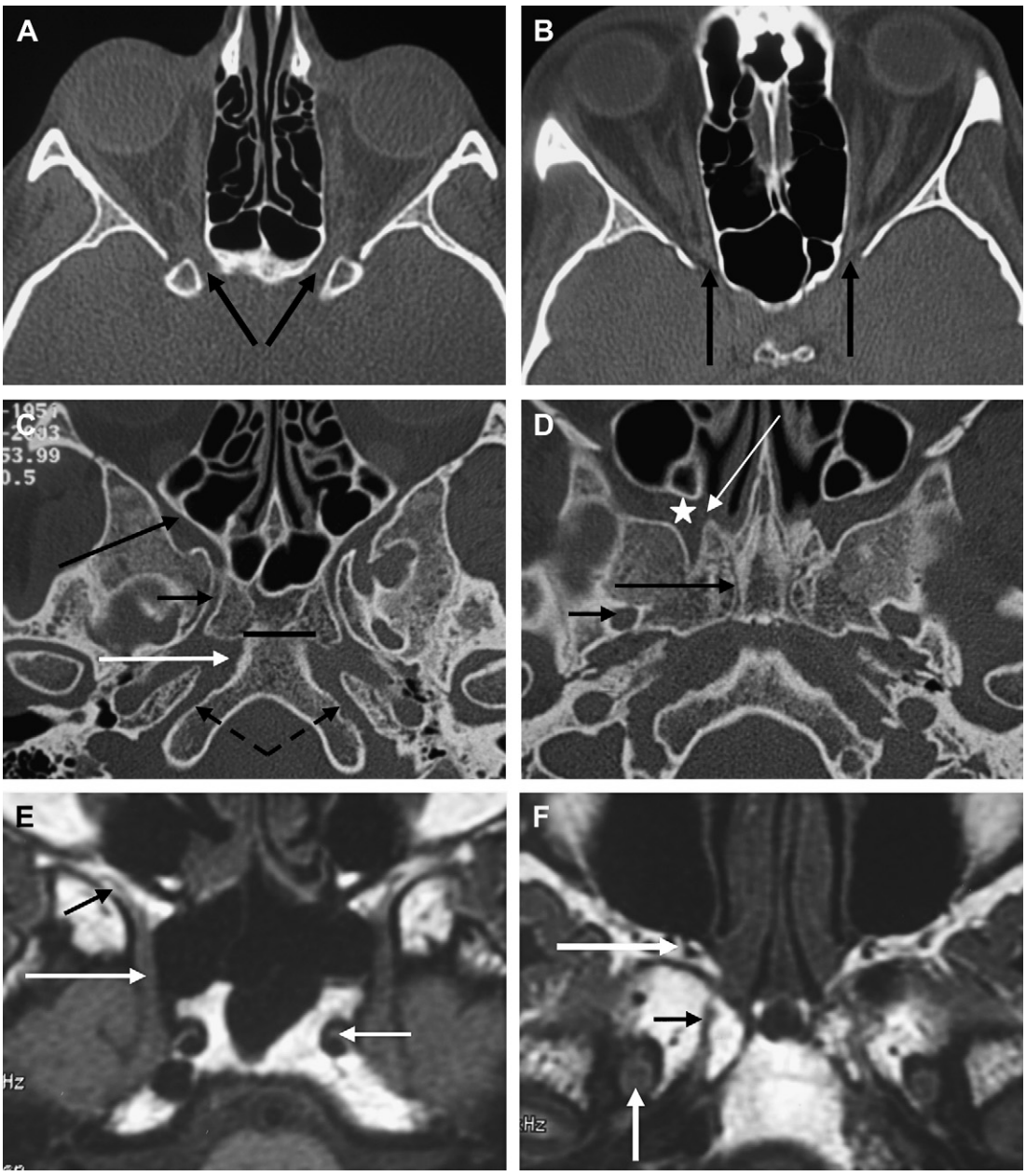

Fig. 4. Axial CT sections in a bone algorithm from superior to inferior show (*A*) the optic canal (*black arrows*); (*B*) the superior orbital fissure (*black arrows*); (*C*) the inferior orbital fissure (*long black arrow*), foramen rotundum (*short black arrow*), foramen lacerum (*white arrow*), the pettroclival (*dashed black arrows*) and spheno-occipital (*black line*) synchondroses; (*D*) the high pterygopalatine fossa (*white star*), the sphenopalatine foramen (*long white arrow*); the vidian canal (*long black arrow*) and foramen ovale (*short black arrow*). Axial sensitivity encoding (SENSE) T1W MR images shows (*E*) V2 within foramen rotundum (*white arrow*), the inferior orbital branch within the inferior orbital fissure (*black arrow*) and (*F*) V3 within foramen ovale (*white arrow*), the vidian nerve (*short black arrow*) and the sphenopalatine ganglion in the high pterygopalatine fossa (*long black arrow*).

IMAGING MODALITIES AND IMAGING TECHNIQUE

In assessing the CSB, CT and MR imaging have a complementary role and are often used together to establish the presumptive diagnosis and to depict the full extent of a lesion.[8] MR imaging is preferred to assess the soft tissue component and to determine its relations with adjacent structures. It is the modality with the highest accuracy

to depict intracranial extent (dural, leptomeningeal, and brain parenchyma invasion), perineural and perivascular spread, and bone marrow involvement.[8,11,12] CT remains the technique of choice to define the bony anatomy of the skull base and to depict the thin cortical margins of skull base neurovascular foramina.[3,8,12,13] It is quite specific in the diagnosis of primary bone lesions (neoplastic and non-neoplastic), is more sensitive than MR imaging in the depiction of calcifications, and can provide information regarding the rate of growth and aggressiveness of a lesion by showing its effect on adjacent bone.[8,13] Whereas permeative and erosive patterns of bone involvement are associated with aggressive rapidly growing lesions, malignant neoplasms, or infectious processes, bone expansion and remodeling with smooth cortical thinning are usually associated with more benign slow-growing processes.[8,9,13]

Therefore, in most institutions with multidisciplinary skull base teams, imaging evaluation of skull base lesions includes a full MR imaging study with gadolinium and a high-resolution CT scan using a bone algorithm during the same visit.[7]

The magnetic resonance protocol should include images in the three orthogonal planes using T1 and T2 weighting, short-tau inversion recovery (STIR), and gadolinium-enhanced T1-weighted images with or without fat supression.[8,11–13] Gradient echo T2* images may be useful to demonstrate the presence of susceptibility artifacts related to the presence of paramagnetic substances, such as calcifications, blood degradation products, or melanin within a lesion.[11,14,15] High-resolution highly T2-weighted sequences (constructive interference in the steady state or driven equilibrium radiofrequency reset pulse) can nicely depict the relation between a lesion and the cisternal course of cranial nerves by showing the nerves as dark structures traveling through the high signal intensity of the cerebrospinal fluid (CSF)–filled cisterns.[12,13] A conventional spin echo or fast spin echo T1-weighted sequence is the single best sequence to depict bone marrow invasion, shown as replacement of the hyperintense fatty marrow by hypointense material.[11–16] Intravenous administration of gadolinium is mandatory to depict meningeal invasion and perineural spread and usually maximizes tumor contrast against adjacent structures that do not enhance to the same degree.[11–15] The use of fat suppression, particularly employing techniques based on frequency-selective fat-suppression pulses, is not consensual. Although it can potentially increase the conspicuity of an enhancing lesion against a fat-containing background, failure of fat suppression attributable to the numerous interfaces seen at the CSB (where bone, air-containing sphenoid sinus, soft tissues, and fat lay close together) is often a problem and may lead to false-positive results.[8,13,17] The use of STIR, which is not based on frequency-selective pulses, or contrast-enhanced T1-weighted images with appropriate windowing is preferred by some.[8,17] High-resolution sensitivity encoding (SENSE) parallel imaging and high-field 3-T MR imaging are being increasingly used to depict fine anatomic detail, particularly to study cranial nerves and the walls of the cavernous sinus.[13,18]

CT studies of the skull base must include images in at least two orthogonal planes with a slice thickness less than 3 mm. Whenever possible, patients should be imaged using a multidetector helical or volumetric scanner, with a single acquisition in the axial plane further reconstructed in different planes as needed without additional radiation to the patient.[8,11] When CT is obtained as an adjunct to a prior contrast-enhanced MR imaging study, orthogonal images in a high-resolution bone algorithm should suffice.[4,7,8] When CT is used as a single examination, a full contrast-enhanced study should be obtained in soft tissue and bone algorithms.[8,16]

CT and open-field MR imaging scanners can be used for image guidance of fine-needle aspiration cytology or core biopsy to obtain a tissue sample for pathologic diagnosis. Magnetic resonance angiography and CT angiography can be powerful adjuncts in the depiction of vascular malformations and in assessing hypervascular lesions.[3,4,8,12]

^{18}F-fluorodeoxyglucose positron emission tomography is essentially used in the follow-up of skull base tumors to differentiate post-treatment changes from persistent or recurrent neoplasm. No routine role has been found in the primary evaluation of patients presenting with CSB lesions, however.[8]

Conventional angiography is mainly used for interventional procedures and to assess the circle of Willis when a carotid artery needs to be sacrificed. Preoperative embolization of hypervascular lesions, such as juvenile nasopharyngeal angiofibromas (JNAs), paragangliomas, a few meningiomas, hemangiopericytomas, and hypervascular metastasis, has greatly reduced surgical mortality and morbidity related to bleeding.[3,4,8–13]

MAJOR IMAGING ISSUES AND DIAGNOSTIC DILEMMAS: HOW TO REPORT A CENTRAL SKULL BASE IMAGING STUDY

To issue a useful imaging report, the radiologist should be aware of the main factors that influence treatment options and may have an impact on the surgical approach.[8] To plan treatment, the

surgeon needs to know the exact location and extent of a skull base lesion to decide whether it can be excised with acceptable morbidity and to choose the best surgical approach and the best route to obtain a biopsy specimen.[3,4,7,8]

Specific contraindications for surgical resection of skull base lesions vary from one institution to another and often among different surgeons.[3,4,7] Usually, they comprise invasion of the lateral or superior walls of the sphenoid sinus, invasion of the cavernous sinus, bilateral optic nerve or optic chiasm involvement, and invasion of the nasopharynx or prevertebral fascia.[3–8]

On every imaging study of the skull base, the radiologist should always report on the amount of bony skull base involvement; on the presence and extent of intracranial and orbital invasion; and on the relation of the lesion to the cavernous sinus, cranial nerves, and vessels, all of which have important implications on treatment planning and prognosis.[3,4,8,12]

Dural invasion is the single most important prognostic factor in skull base tumors.[19–21] Whereas an extradural lesion can be resected by means of an inferior ENT approach, a lesion that has transgressed the dura requires a combined craniofacial approach and is associated with a significant decrease in the 5-year survival rate and the specific disease-free interval.[8,19–21] Contrast-enhanced MR imaging is the best imaging modality to depict dural invasion.[8,12,13] Imaging signs of dural invasion in decreasing order of positive predictive value include contrast enhancement or edema of the brain parenchyma adjacent to tumor, leptomeningeal enhancement, nodular dural enhancement, and linear dural enhancement thicker than 5 mm.[8,19–21] Dural enhancement less than 5 mm is the most sensitive but least specific of all imaging signs because it can result from fibrovascular changes and does not necessarily indicate dural invasion.[8,13]

Orbital involvement is another important issue in surgical planning. The most common site of orbital invasion by CSB lesions is by way of the orbital fissures or orbital apex (**Fig. 5**D). Loss of fat and abnormal enhancement within these neural foramina indicate invasion.[8,11,12,22] Because of the close relation between the periorbita and the dural sheath of the optic nerve, involvement of the orbital apex by a skull base lesion usually requires orbital exenteration with sacrifice of the optic nerve.[8,9]

Invasion of the cavernous sinus usually precludes complete resection of a lesion. Imaging signs of cavernous sinus invasion include compression, encasement, stenosis, or irregularity of the cavernous carotid artery; loss of contrast enhancement of the cavernous sinus, which is best depicted on a dynamic coronal MR imaging study; and bulging of the lateral sinus wall, which is concave under normal conditions (see **Fig. 5**E, F).[8,9,11–13,18] When subtle, cavernous sinus invasion may be hard to depict, even using optimal technique. Because the dural leaflets are not clearly visible, it is often difficult to differentiate a bulge of the sinus walls because of compression by an extrinsic lesion from actual dural transgression. The use of 3-T MR imaging scanners seems promising in solving this issue. It should also be kept in mind that the cavernous sinus may be affected by interdural lesions laying within the dural leaflets of the lateral wall or by true intracavernous lesions. Whereas the former tend to displace the cavernous carotid artery without encasement or stenosis, the latter tend to encase and narrow its lumen.[3,4,12,18]

PATHOLOGIC FINDINGS

Most patients with CSB problems present with headache, cranial nerve deficits, proptosis, Eustachian tube dysfunction, or other symptoms related to the nasopharyngeal airway.[8,11–15] Because clinical examination of the CSB is limited, surgeons often have to rely on imaging studies to reach a diagnosis and plan subsequent treatment.

The following description of CSB lesions is based on a radiologist's friendly approach and on the frequency and propensity for certain disease processes to occur at specific sites. Lesions that are not site specific, originating from the bony skull base, such as fibro-osseous conditions and primary and secondary bone tumors, are discussed at the end of this article.

Midline Sagittal Central Skull Base Lesions

Midline sagittal CSB lesions comprise lesions arising from the sphenoid body, sphenoid sinus, and clivus; from the sella turcica immediately above; and from the nasopharynx immediately below (see **Fig. 3**). Whereas lesions arising within the sella turcica tend to displace the sellar floor inferiorly, intrinsic lesions of the clivus and those arising from the nasopharynx tend to push the sellar floor and pituitary gland superiorly.[2,4,9,12]

Lesions of the sphenoid sinus can be inflammatory and neoplastic. Chronic obliteration of sinus drainage may lead to mucocele formation. Sphenoid mucoceles, as is the case with those seen elsewhere, present as expansile lesions thinning and remodeling the sinus walls and eventually leading to cortical bone dehiscence.[9,10] This tumor, made of retained secretions, may show variable density and signal intensity on imaging studies depending on the degree of hydration, protein concentration,

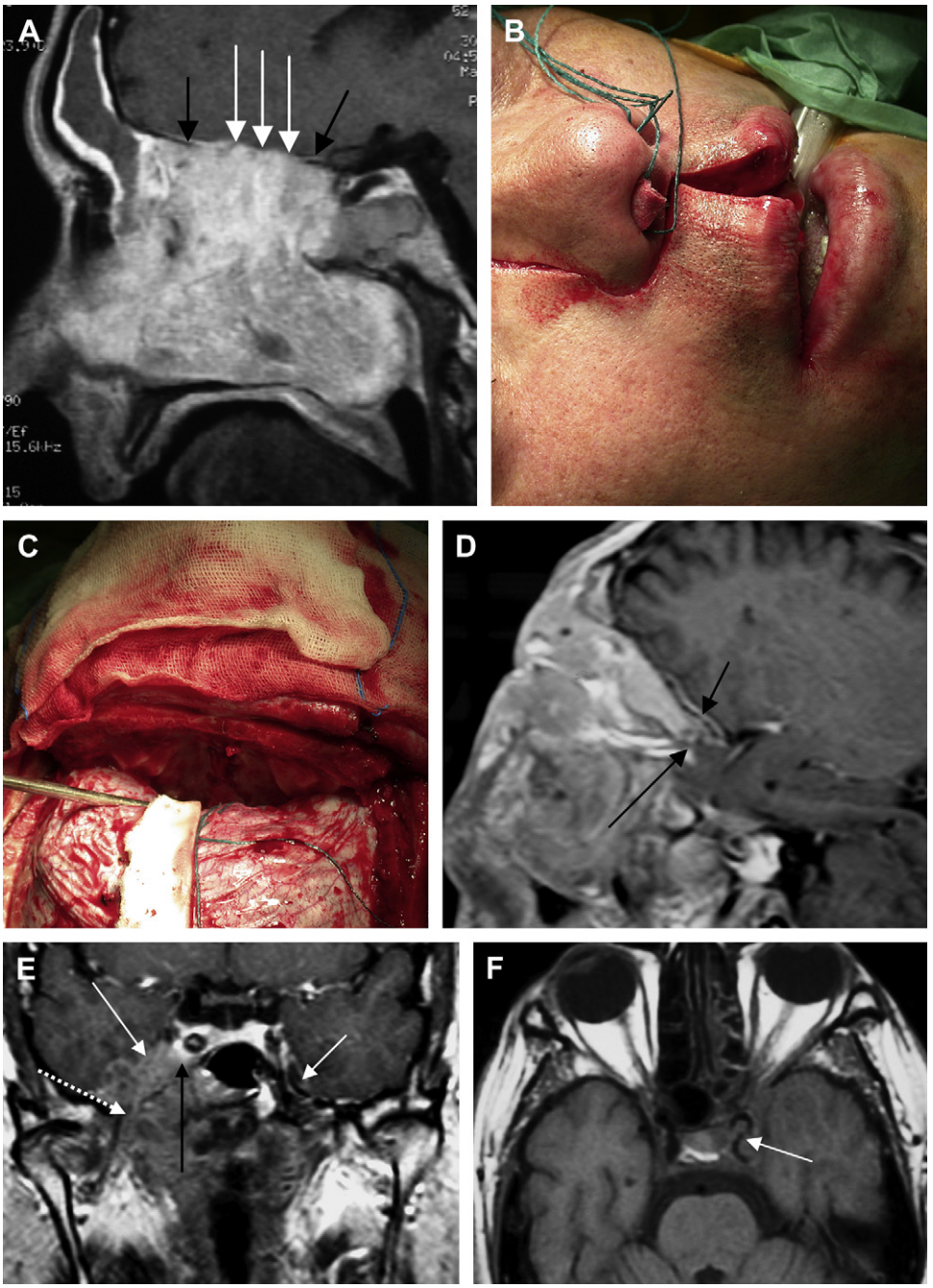

Fig. 5. (*A*) Gadolinium-enhanced sagittal T1-weighted MR imaging shows a large enhancing sinonasal neoplasm transgressing the skull base at the level of the planum sphenoidale. Note the discontinuity of the thin enhancing line corresponding to the dura (*black arrows*) with small areas of tumoral enhancement effacing the adjacent subarachnoid space (*white arrows*), reflecting transdural growth (pathologically proved). No brain edema or enhancement is seen to suggest invasion of the parenchyma. Images of a combined craniofacial resection: paranasal ear, nose, and throat approach (*B*) and bifrontal neurosurgical approach (*C*). (*D*) Gadolinium-enhanced sagittal T1-weighted image shows another sinonasal mass with orbital invasion and posterior extension into the orbital apex (*long black arrow*). Also note the smooth linear dural enhancement along the floor of the anterior cranial fossa (*short black arrow*), suggesting reactive fibrovascular changes. (*E*) Gadolinium-enhanced coronal T1-weighted image demonstrates a nasopharyngeal mass with infiltrative borders transgressing the CSB. Note the partial obliteration of the left cavernous sinus enhancement (*long black arrow*) and outward bulging of its lateral wall (*long white arrow*). Also, note tumor growth along V3, back to the foramen ovale (*dashed white arrow*), with complete obliteration of Meckel's cave (note the Meckel's cave on the normal side; *short white arrow*). (*F*) Axial T1-weighted image shows irregularity and stenosis of the right cavernous carotid artery (*white arrow*) attributable to a mass lesion invading the cavernous sinus and orbital apex.

and presence of calcification or fungal colonization (mycetoma) and does not enhance after intravenous administration of contrast material, except for a thin peripheral rim corresponding to the sinus mucosa (**Fig. 6**). The imaging appearance is that of a benign slow-growing lesion, and the diagnosis is usually straightforward in the absence of complications.[9,10,14,15]

Primary neoplasms of the sphenoid sinus are quite rare, because the sphenoid is most often secondarily invaded by tumors originating elsewhere.[3,4,10] Tumor histologic findings are similar to those seen in other paranasal sinuses, with squamous cell carcinoma being the most common.[3,10]

Clivus lesions include hematogenous bone metastasis, plasmacytoma or multiple myeloma, primary bone tumors, chordoma, and chondrosarcoma.

Clival chordoma is a benign locally invasive neoplasm originating from embryonic remnants of notochord that become entrapped within the basisphenoid, accounting for its typical midline sagittal location.[14,15,23,24] Seldom can it be seen in the nasopharynx or in the intracranial compartment.[23,24] Chordomas present as expansile lytic lesions, often with an aggressive pattern of bone destruction. MR imaging can nicely depict the replacement of the fatty marrow of the clivus by a hypointense tissue mass on plain sagittal T1-weighted images. Density and signal intensity are variable because of the presence of hemorrhage, cystic or myxoid components, calcification, and fragments of trabecular bone that become engulfed within the tumor mass.[9,23,24] After contrast, a lobulated pattern of enhancement is usually described (**Fig. 7**).[9,14,15,23,24]

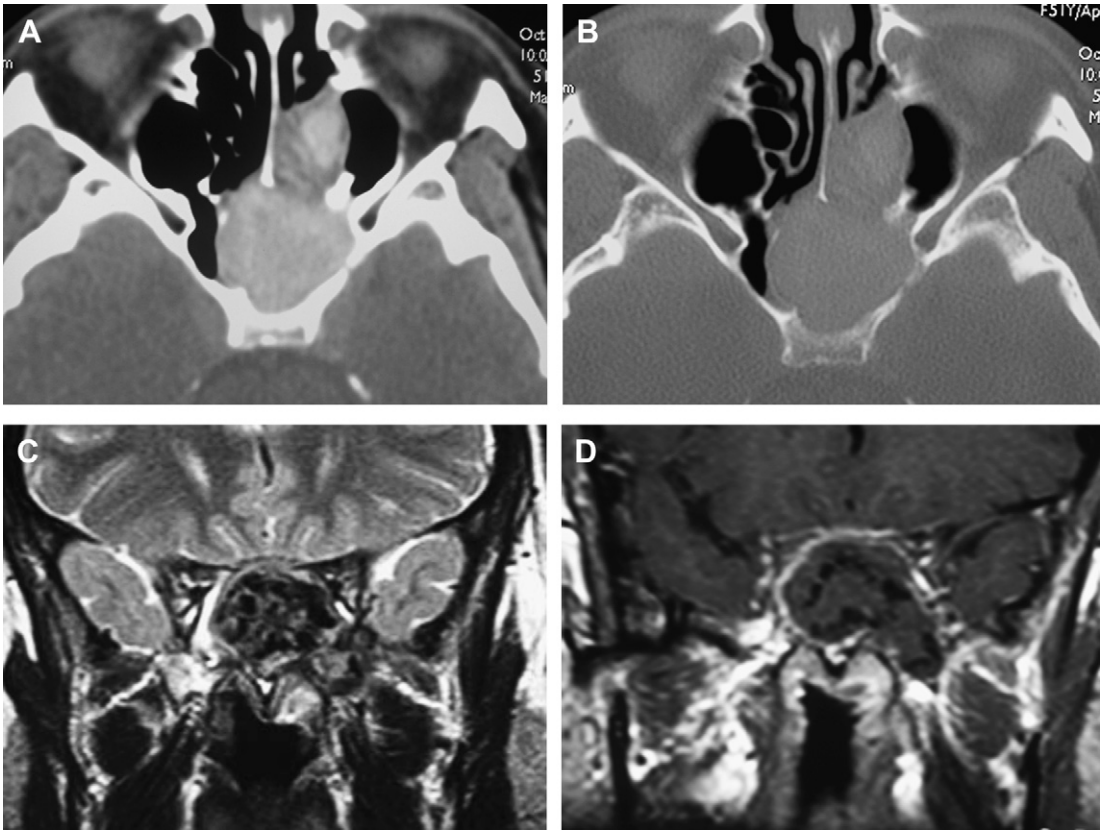

Fig. 6. Axial CT scan in soft tissue (*A*) and a bone algorithm (*B*) shows a heterogeneous but mostly spontaneous hyperdense mass filling in and expanding the right sphenoid sinus and posterior ethmoid cells. Note the thinning and remodeling of the bony walls of the sphenoid sinus without elements of frank destruction, suggestive of a slow-growing process. Corresponding MR imaging, coronal T2-weighted image (*C*) and gadolinium-enhanced coronal T1-weighted image (*D*), show that the material filling in the sinus is markedly heterogeneous, predominantly of low signal intensity on T2-weighted images, with serpiginous areas of signal void. Only peripheral enhancement is noted after gadolinium administration (sphenoid sinus mucocele superinfected by fungal hypha-mycetoma).

Sellar lesions that may invade the CSB include mainly macroadenomas and, in a far distant second place, craniopharyngiomas.[3,4,9] Pituitary macroadenomas tend to fill and expand the sella; may remodel the sellar floor and dorsum sella; extend superiorly into the suprasellar cistern through the diaphragm sella; and expand laterally into the cavernous sinus, wherein they can displace or encase the cavernous carotid artery without narrowing its lumen.[3,4,8] Invasive macroadenomas can breach the sellar floor and clivus and may extend into the sphenoid sinus.[3,4,9] Occasionally, pituitary macroadenomas are completely intraosseous and may cause a diagnostic dilemma. Sagittal and coronal MR imaging is particularly helpful in making the diagnosis. Diagnostic clues include the presence of an empty sella; off-midline deviation of the pituitary stalk; and the presence of an intact sellar floor, often displaced inferiorly, differentiating pituitary macroadenomas from lesions arising primarily from the clivus or from the sphenoid sinus (**Fig. 8**).[9,12]

Craniopharyngiomas are histologically benign lesions originating from embryonic remnants of the pharyngohypophyseal canal or Rathke's pouch.[3,4,9] They can be seen anywhere from the nasopharynx to the hypothalamus, with the most common location being suprasellar.[3,4,11,12] When completely intraosseous within the sphenoid, they may be hard to diagnose. Typically, craniopharyngiomas are largely cystic or mixed tumors, often showing calcifications.[3,4,11,12] The solid component enhances after intravenous contrast administration (**Fig. 9**).

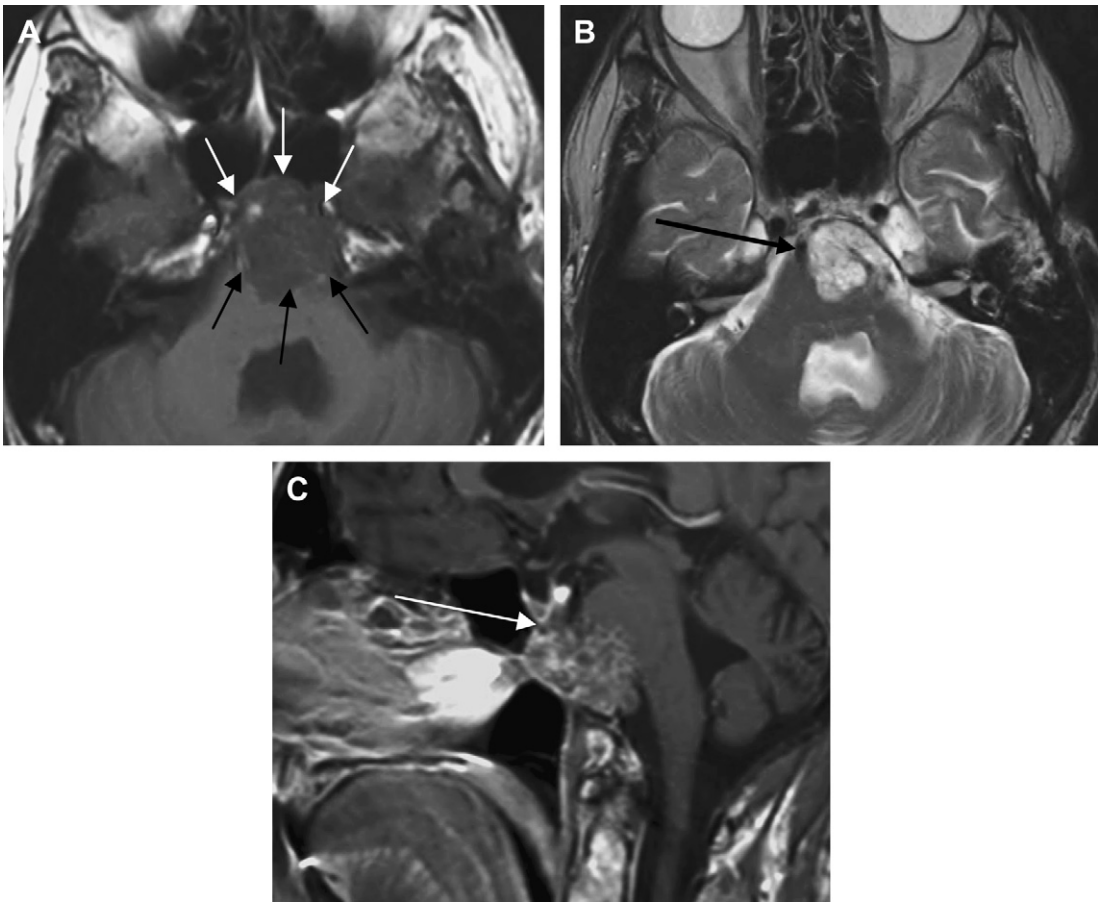

Fig. 7. Axial T1-weighted (*A*), T2-weighted (*B*), and gadolinium-enhanced sagittal T1-weighted (*C*) images show a mass lesion expanding and replacing the fatty marrow of the clivus, with frank destruction of the superior cortical margin. The lesion extends into the posterior cranial fossa, obliterates the prepontine cistern, displaces the basilar artery to the right (*long black arrow in B*), and compresses the ventral pons (*short black arrows in A*). Anteriorly, it bulges into the sphenoid sinus (*small white arrows in A*), and, superiorly, it stops at the sellar floor (*long white arrow in C*). The lesion is of intermediate signal intensity on T1-weighted imaging and hyperintense on T2-weighted imaging, with a faint trabecular pattern, and shows lobulated honeycombed-like enhancement (clival chordoma).

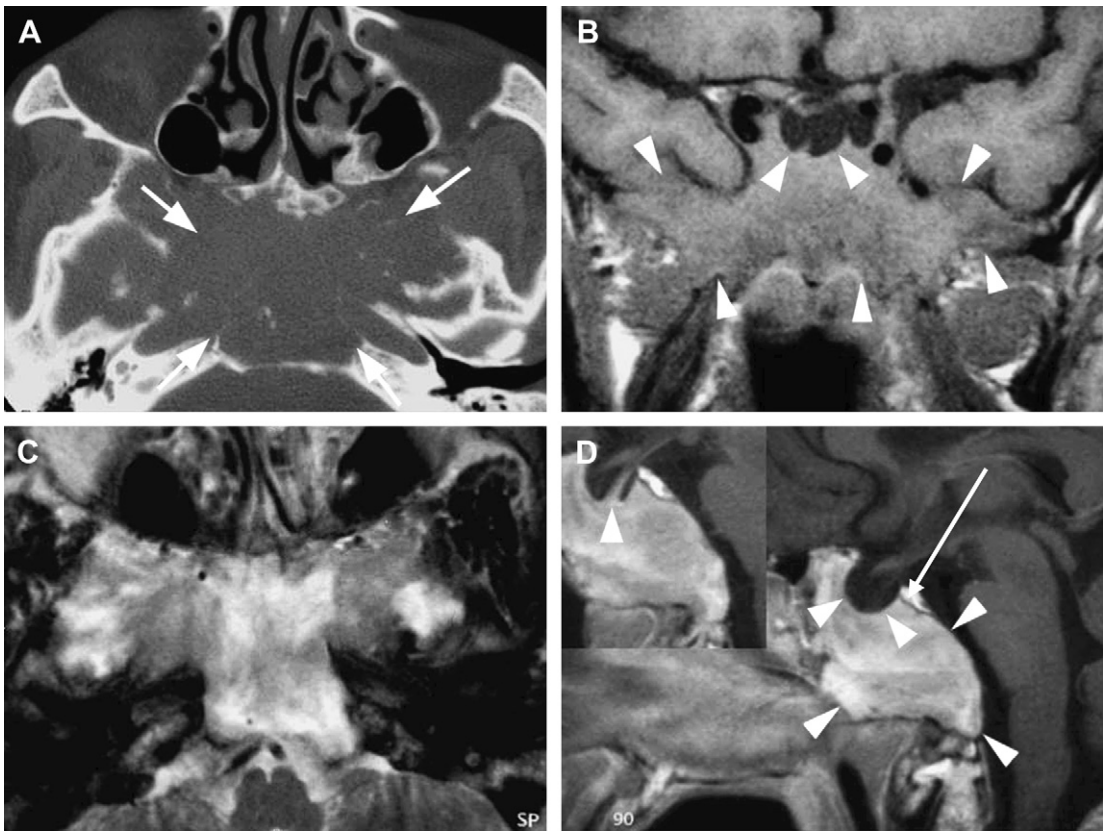

Fig. 8. Axial CT scan in a bone algorithm shows a large destructive lesion almost entirely replacing the sphenoid bone (*A*), retaining its original shape and with small bony fragments engulfed within the lesion (*white arrowheads in B*). Coronal T1-weighted (*B*) and contrast-enhanced sagittal T1-weighted (*D*) MR images show to advantage the soft tissue mass delineating the sphenoid (*white arrowheads*). Note the presence of an empty sella (*black arrowheads*), the inferior displacement of the sellar floor, and the rightward deviation of the pituitary stalk. The high signal intensity of the neurohypophysis can be seen in a normal anatomic location (*long white arrow in D*). (*C*) On T2-weighted imaging, the lesion is heterogeneous in signal intensity but predominantly hyperintense (intra-osseous pituitary adenoma).

Meningiomas of the sellar and parasellar regions account for 20% to 25% of all meningiomas.[3,4,7] The most common sites of origin include the planum sphenoidale, tuberculum sella, clinoid processes, and sellar diaphragm.[3,4,7] They present as broad dural-based masses and are isointense to gray matter, enhancing vividly and homogeneously after contrast administration, often showing a dural tail.[3,4,10–12] Sellar meningiomas tend to push and compress the pituitary gland against the sellar floor (**Fig. 10**). Associated hyperostosis with upward blistering of the planum sphenoidale and tuberculum sella and pneumosinus dilatans are typical features that can be nicely depicted on CT and MR imaging scans.[3,4,9–12]

Nasopharyngeal lesions, infectious and neoplastic, may affect the CSB from below. Because of the tough buccopharyngeal and pharyngobasilar fascias, tumor spread is usually directed superiorly against the clivus and foramen lacerum (**Fig. 11**).[22,25] It should be kept in mind that nasopharyngeal cancers can occasionally be completely submucosal, presenting with extensive CSB destruction and only a slight bulge in the nasopharyngeal mucosal space with normal overlying mucosa.[9,22,25] In this case, deep transnasal biopsies are required to make the diagnosis.

Parasagittal Central Skull Base Lesions

Parasagittal CSB lesions originate from the greater sphenoid wing, cavernous sinus, cranial nerves traversing the neurovascular foramina, and petroclival synchondrosis. Developmental lesions, such as basal transsphenoidal cephaloceles, may also be seen.

Cavernous sinus lesions include primary and secondary cranial nerve tumors; vascular malformations; meningiomas; and inflammatory conditions, such as neuritis and Tolosa-Hunt syndrome.

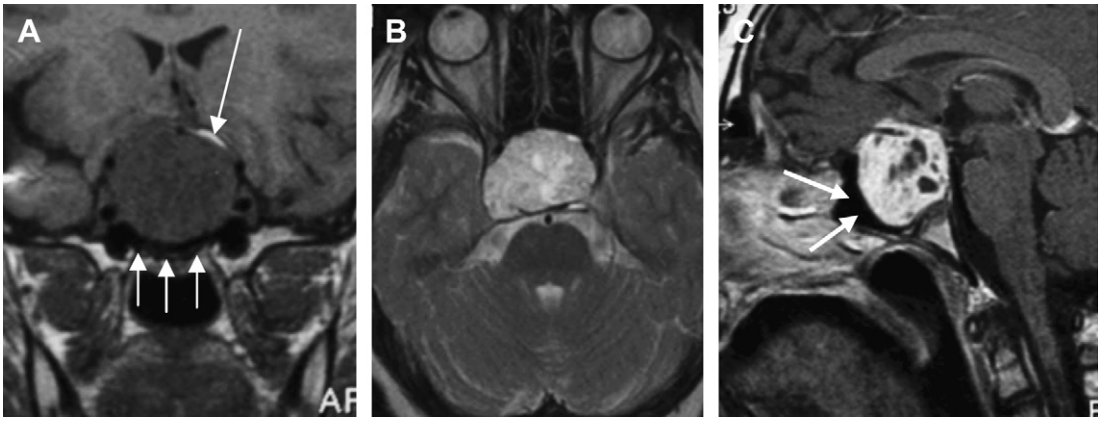

Fig. 9. Coronal T1-weighted (*A*), axial T2-weighted (*B*) and gadolinium-enhanced sagittal T1-weighted (*C*) images show a rounded well-marginated mass lesion, expanding the sella and growing into the suprasellar cistern. Note the inferior displacement of the sellar floor, almost collapsing the sphenoid sinus (*small white arrows in A and C*). The lesion is of intermediate signal intensity on T1-weighted and T2-weighted images with small T2-weighted hyperintense and nonenhancing cystic areas. Also, note a thin spontaneously hyper-intense rim on the coronal T1-weighted image suggesting marginal calcification (*long white arrow in A*) (craniopharyngioma).

Peripheral nerve sheath tumors (PNSTs) tend to follow the axis of the nerve of origin, and the diagnosis is straightforward once the anatomic course of the nerve is recognized.

Schwannomas and neurofibromas are the most common lesions and can affect virtually any cranial nerve. Schwannomas present as well-defined soft tissue masses of low signal intensity on T1-weighted MR imaging and have intermediate to high signal on T2-weighted MR imaging, moderately enhancing after gadolinium administration.[9,12,14,15,26,27] Large tumors tend to show cystic or necrotic areas, and peripheral CSF cysts can also be seen.[14,15,26,27] Fatty degeneration can occur in long-standing neurofibromas, accounting for low density on CT and T1-weighted hyperintensity on MR imaging.[14,15,26,27] These benign slow-growing neoplasms tend to remodel rather then erode adjacent bone, and when extending peripherally, they produce smooth enlargement of the exiting skull base neural foramina (**Fig. 12**).[14,15,25–27] Neurofibromas can occur as isolated lesions or as part of neurofibromatosis type I.[14,15,26,27] Malignant PNSTs, however, are most commonly associated with neurofibromatosis type 1.[9,15,27] These are more aggressive infiltrative lesions that spread diffusely along peripheral branches and show ill-defined borders.[26,27]

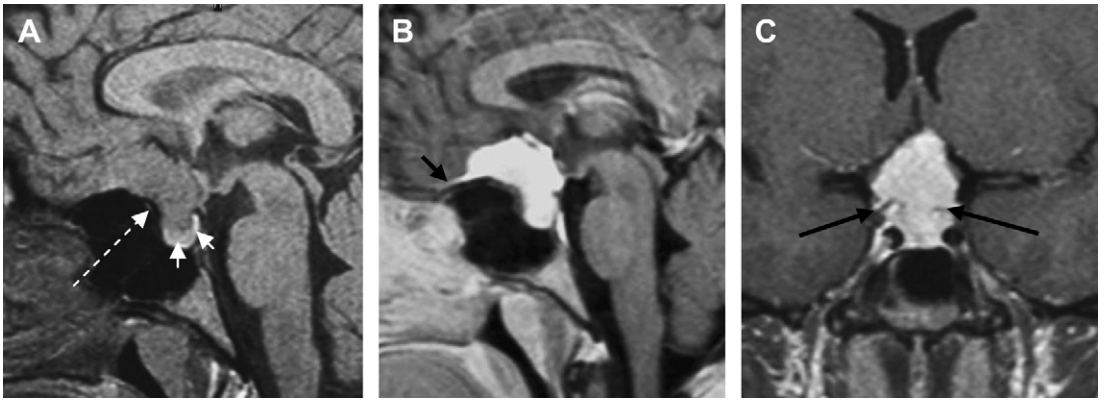

Fig. 10. Sagittal T1-weighted image (*A*) and gadolinium-enhanced sagittal (*B*) and coronal (*C*) T1-weighted images show a dural-based lesion along the posterior aspect of the planum, transgressing the diaphragm and growing into the sella, compressing the pituitary gland against the sellar floor (*small white arrows in A*). Note the hourglass shape of the lesion, which is best appreciated on the coronal plane, with a stricture at the sellar diaphragm (*black arrows in C*). The lesion is isointense with gray matter and enhances homogeneously, showing a thin dural tail along the planum (*small black arrow in B*). Bone sclerosis, with blistering of the sphenoid roof (*dashed white arrow in A*) and pneumosinus dilatans, can also be seen (sphenosellar meningioma).

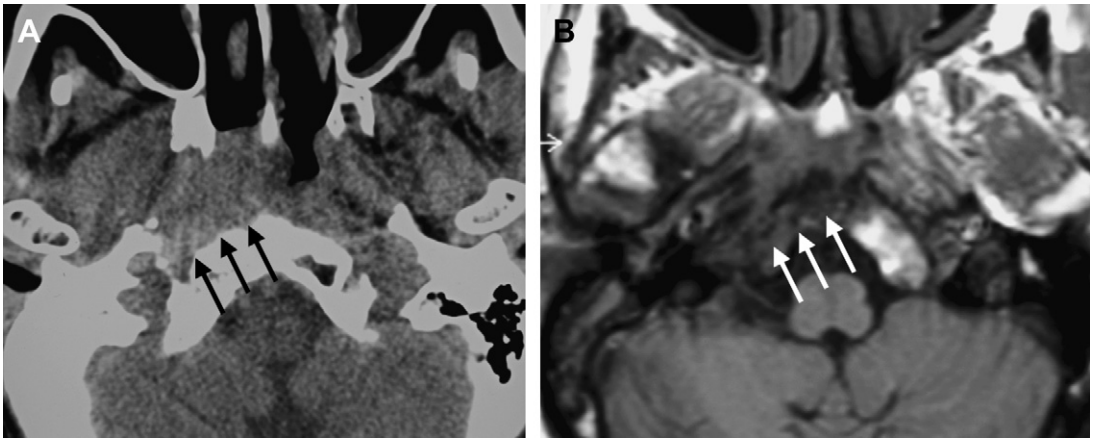

Fig. 11. Plain axial CT scan (*A*) and axial T1-weighted MR image (*B*) show a mass lesion in the posterolateral wall of the nasopharynx obliterating the fossa of Rosenmüller, effacing the parapharyngeal fat, and growing posteriorly into the jugular foramen. Note the sclerosis and slight irregularity of the cortical margin of the right lateral aspect of the clivus on the CT image (*black arrows*) corresponding to replacement of the fatty marrow, which is best appreciated on MR imaging (*white arrows*).

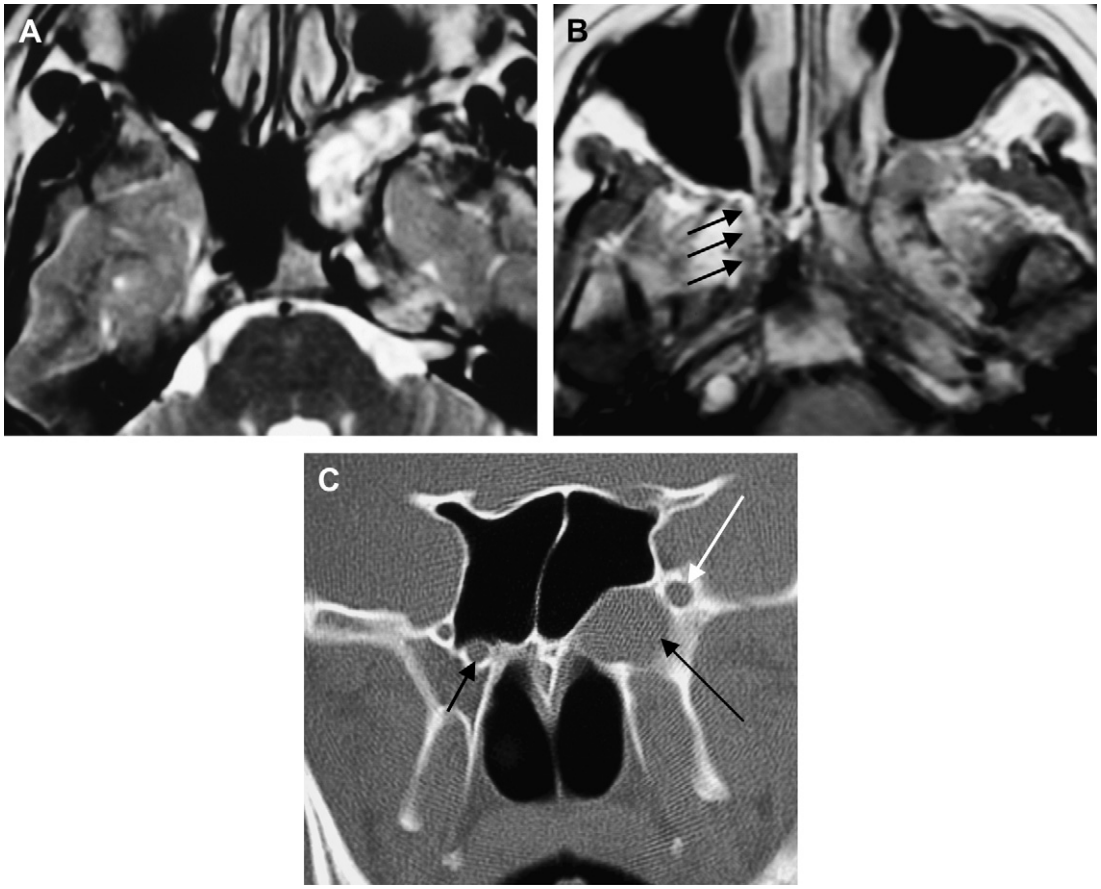

Fig. 12. Axial T2-weighted (*A*) and gadolinium-enhanced T1-weighted (*B*) images show a sausage-shaped lesion extending from the foramen lacerum posteriorly into the high pterygopalatine fossa anteriorly, following the course of the vidian nerve. (*C*) Coronal CT image in the bone algorithm shows the smooth enlargement of the vidian canal (*long black arrow*) and superior displacement of the foramen rotundum (*white arrow*). Note the vidian nerve on contralateral side (*short black arrows* on *B* and *C*).

The most commonly affected cranial nerve in the CSB is the trigeminal nerve. [26–28] The cranial nerves can also be affected by anterograde or retrograde spread of head and neck malignancies, a phenomenon known as perineural spread.[22,26,29] It manifests as focal or segmental enlargement and abnormal enhancement along the course of a cranial nerve, often with skip areas.[14,15,26,29] This type of spread is most often seen with squamous cell carcinoma, the most frequent neoplasm of the head and neck, but can also be seen with salivary gland malignancies (mainly adenoid cystic and mucoepidermoid carcinomas), hematologic malignancies, and melanoma.[26,29] On CT, perineural spread can be depicted by enlargement of the skull base neural foramina of the affected nerve, by effacement of the foraminal fat, or indirectly through denervation atrophy of the muscles supplied by a particular nerve.[14,15,26,29] MR imaging is more sensitive, allowing earlier detection of this type of spread.[9,12,26,29] Plain T1-weighted images and fat-suppressed contrast-enhanced T1-weighted images are particularly well suited to detect perineural spread through effacement of neuroforaminal fat and areas of focal or segmental enhancement (**Fig. 13**).[26,28,29] Cranial nerve neuritis can have the exact same appearance on imaging; therefore, the clinical setting is crucial to achieve a correct diagnosis (**Fig. 14**). In most cases, neuritis results from viral infection secondary to herpes simplex, herpes zoster, cytomegalovirus, or HIV, to mention the most common infections.[14,15,26,29]

Pyogenic and fungal infections originating from the orbit, nasopharynx, and paranasal sinuses may access the cavernous sinus, spreading along neurovascular structures. Skull base osteomyelitis, abscess formation and cavernous sinus, and

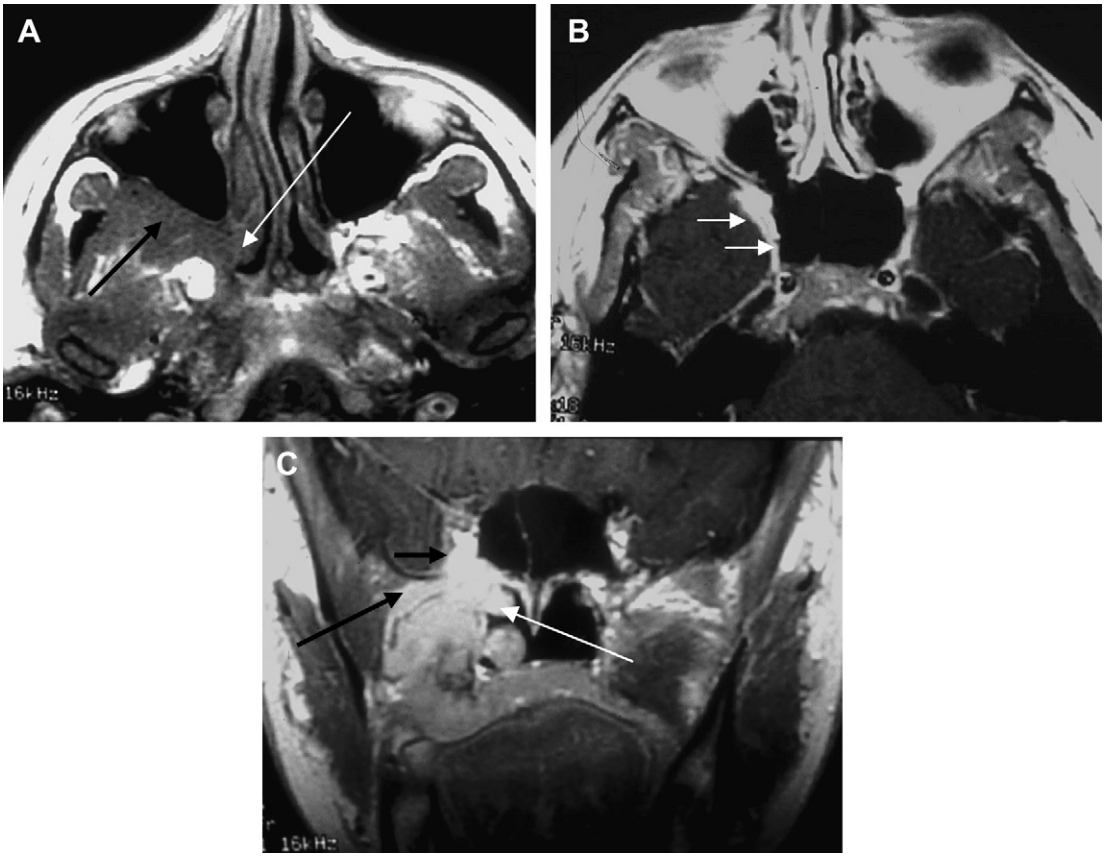

Fig. 13. (*A*) Axial T1-weighted image shows a soft tissue mass in the right pterygopalatine fossa growing medially into the posterior nasal cavity through the sphenopalatine foramen (*long white arrow*) and laterally into the infratemporal fossa and retroantral fat through the pterygomaxillary fissure (*long black arrow*). Postgadolinium axial (*B*) and coronal (*C*) T1-weighted images demonstrate abnormal enhancement of V2 along the foramen rotundum back to the cavernous sinus (*short white arrows in B*). Also, note the enlargement of the inferior cavernous sinus (*short black arrow in C*), tumor growth into the posterior nasal cavity through the sphenopalatine foramen (*long white arrow*) and laterally, into the infratemporal fossa via the pterygomaxillary fissure (*long black arrow*).

superior ophthalmic vein thrombosis are potential complications best demonstrated by magnetic resonance imaging.[3,4,9,12]

Inflammatory pseudotumor of the cavernous sinus and orbital apex, Tolosa-Hunt syndrome, is a diagnosis of exclusion after all infectious and specific inflammatory conditions, particularly sarcoidosis, have been ruled out.[26,28] It is characterized by painful ophthalmoplegia with deficits of cranial nerves III, IV, V1, and VI and a prompt response to steroid therapy.[3,15,26] MR imaging is the modality of choice, showing abnormal enhancing soft tissue within the cavernous sinus and orbital apex, often extending along the floor of the middle cranial fossa, and, occasionally, irregular narrowing of the cavernous carotid artery.[15,26] This tissue tends to be isointense to muscle on T1-weighted images and of low to intermediate signal intensity on T2-weighted images (**Fig. 15**).[12,15,26]

Cavernous sinus vascular malformations, including aneurysms, carotid-cavernous fistulas, and hemangiomas, are all associated with focal or diffuse enlargement of the cavernous sinus with outward bulging of its lateral wall; when long standing, they can also lead to remodeling of the inner wall of the sphenoid sinus.[3,4,9,26] These are imaging diagnoses that should be ruled out before any attempts to obtain tissue diagnosis are made.

Giant cavernous carotid aneurysms present as expansile lesions of the cavernous sinus with variable signal characteristics.[3,4,9,12] When the aneurysm lumen is completely patent, a fusiform or saccular flow void on MR imaging is the rule. When a varying amount of thrombosis is present, signal intensity is heterogeneous, reflecting the presence of blood products in different stages of degradation, calcifications, and flowing blood (**Fig. 16**).[9,11,12] The presence of flow-related

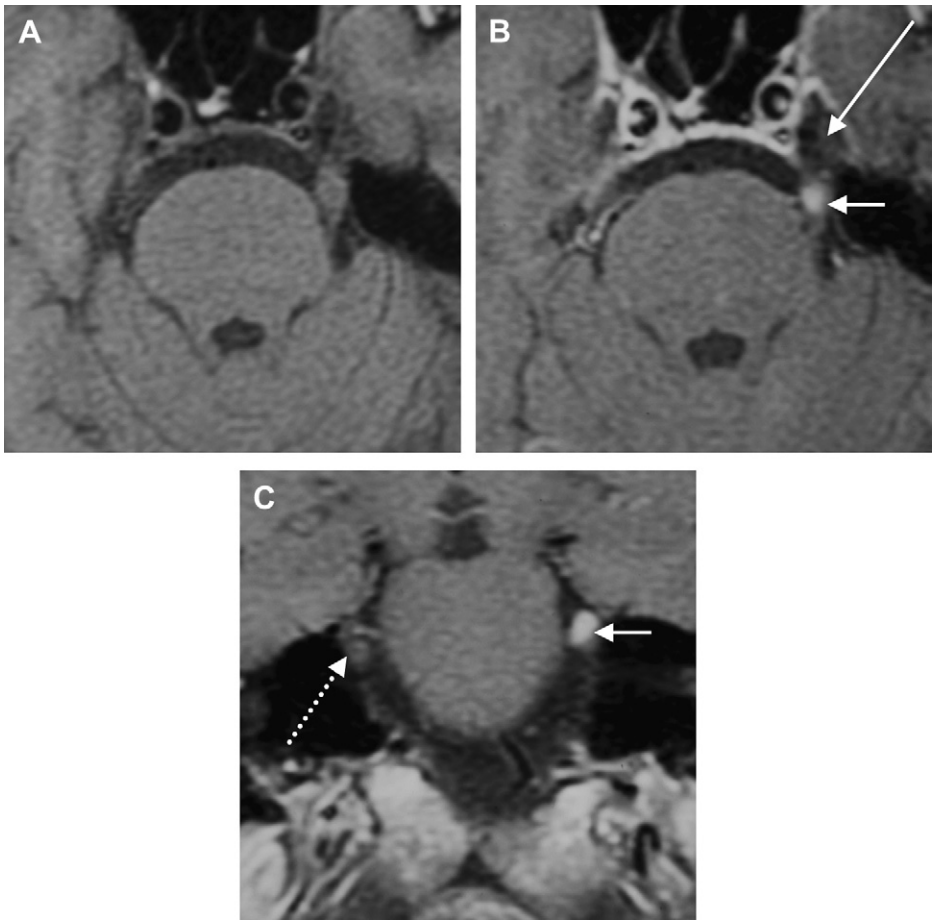

Fig. 14. Axial T1-weighted image (*A*) and postgadolinium axial (*B*) and coronal (*C*) T1-weighted images show a small focus of enhancement and slight enlargement of the cisternal segment of the left trigeminal nerve (*short white arrows*), which does not extend into Meckel's cave (*long white arrow in B*). Note the cisternal segment of the right trigeminal nerve (*dashed white arrow in C*). (This focal enhancement disappeared on follow-up scans, and a presumptive diagnosis of neuronitis was made).

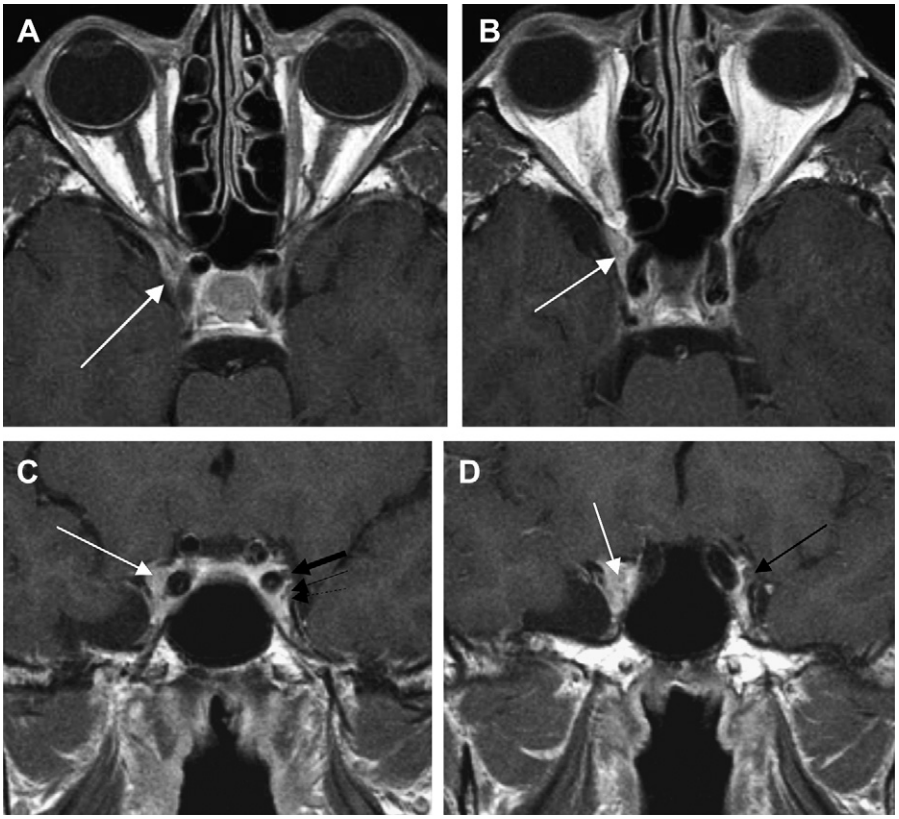

Fig. 15. Post-gadolinium (*A and B*) and coronal (*B and C*) T1W MR images demonstrate soft tissue thickening and abnormal enhancement in the lateral wall of the right cavernous sinus, superior orbital fissure and optic canal (*long white arrows in A–C*). In (*C*) note cranial nerves III (*thick black arrow*), IV (*thin black arrow*), and V1 (*dashed black arrow*) in the lateral wall of the cavernous sinus on the left side, from superior to inferior. (*D*) On the affected side the nerves are enhancing and can hardly be recognized within the enhancing sinus (enhancing oculomotor nerve- *short white arrow*) (Tolosa-Hunt syndrome).

artifacts on the phase-encoding axis may be a clue to the diagnosis. Whereas recent thrombus containing deoxihemoglobin and intracellular methemoglobin layers close to the patent lumen, old thrombus containing extracellular metahemoglobin and hemosiderin tends to layer at the periphery.[9,11,12] On CT, a potential pitfall is to mistake a largely patent aneurysm for a cavernous sinus meningioma when a CT angiogram is not performed. Angio-CT or angio-MR imaging should be used to confirm the diagnosis and clearly delineate the aneurysm.[9,12]

Sphenocavernous and petroclival meningiomas are the most common neoplasms affecting the parasagittal CSB, originating from the intracranial compartment (**Fig. 17**). Cavernous meningiomas lead to bulging of the lateral wall of the cavernous sinus and can grow laterally along the floor of the middle cranial fossa, anteriorly into the superior orbital fissure and orbital apex, medially into the sphenoid sinus and sella, posteriorly into Meckel's cave and posterior cranial fossa, and inferolaterally into the masticator space along the foramen ovale (mimicking a trigeminal nerve schwannoma).[9,12,14,15] Intradiploic growth into the body of the sphenoid and clivus is not infrequent. These lesions tend to follow the signal intensity of gray matter in all imaging sequences and to enhance vividly and homogeneously after administration of gadolinium.

Cephaloceles of the parasagittal CSB are of rare occurrence and consist of herniation of the intracranial contents (meninges or brain parenchyma) through a skull base defect in the greater sphenoid wing into the masticator space immediately below (**Fig. 18**).[3,4,9,12] Coronal and sagittal imaging is helpful in establishing this imaging diagnosis. An unaware biopsy may lead to a CSF fistula and meningitis.

Chondroid tumors, chondromyxoid fibroma, and low- and high-grade chondrosarcomas originate from cartilaginous remnants of the skull base synchondroses, most commonly from the petroclival synchondrosis, accounting for the off-midline parasagittal location of these

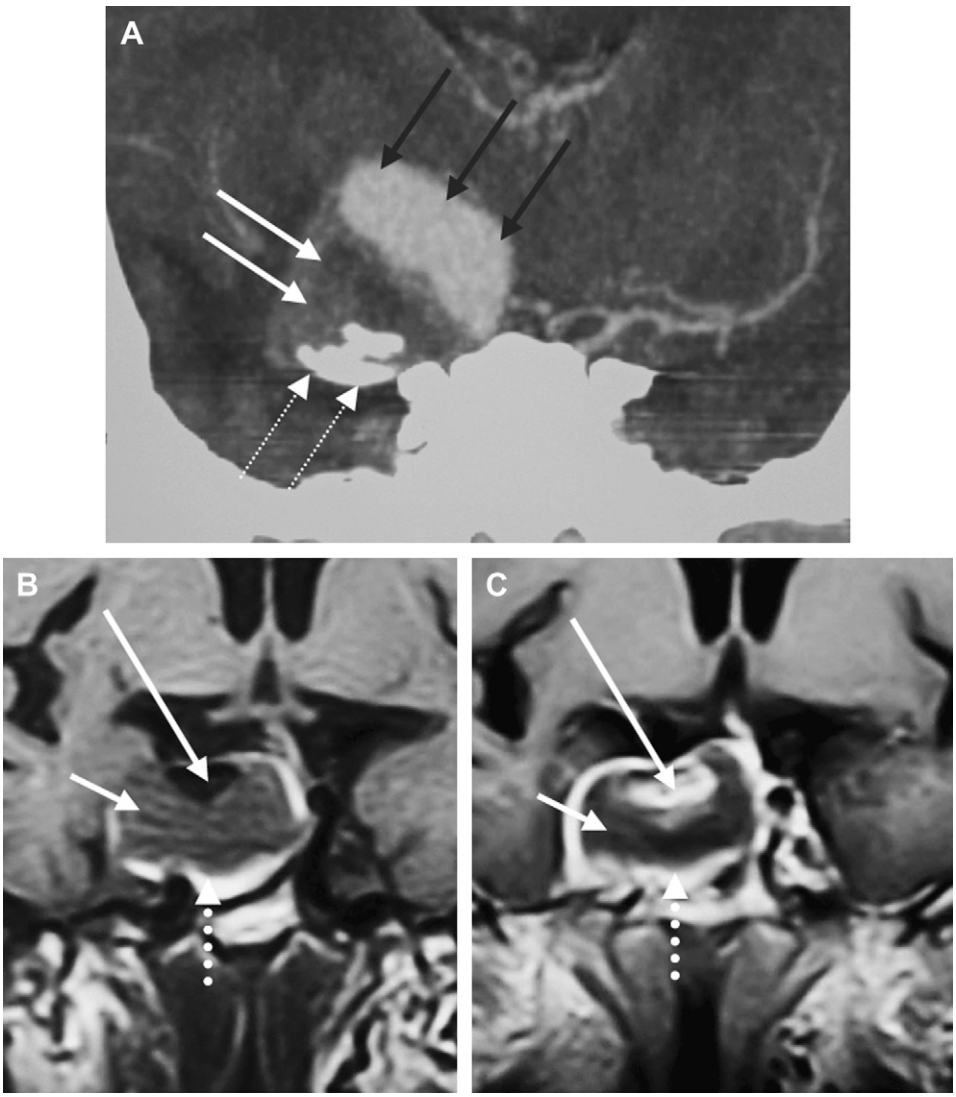

Fig. 16. Coronal CT reconstruction from a CT angiogram (*A*) demonstrates a giant cavernous carotid aneurysm shown as a complex lesion in the right cavernous sinus and supraclinoid region, with an area of early enhancement which corresponds to the patent lumen (*black arrows*) and a non-enhancing hypodense area suggesting thrombus (*white arrows*). Also noted are extensive, layered atheromatous calcifications (*white dashed arrows*). Coronal pre-gadolinium (*B*) and post-gadolinium (*C*) T1W MR images (on another patient) show a complex lesion in the right cavernous sinus at the expected location of the cavernous carotid artery. The lesion has an eccentric flow void enhancing after gadolinium, corresponding to the patent arterial lumen (*long white arrows in C–D*), hypointense material consistent with early clot (*short white arrows*) and, at the periphery, spontaneous T1 hyperintensity, suggesting the presence of metahemoglobin (*white dashed arrows*). (Cavernous carotid artery aneurysm).

neoplasms.[9,14,15,30–32] Chondroid type calcifications are typical for these tumors and are best appreciated on CT.[9,30–32] On MR imaging, high signal intensity on T2-weighted images, often higher than that of CSF, is also a distinctive feature.[9,15,30–32] The signal intensity of calcifications is variable depending on the size and composition of calcium crystals.[15,30–32] Cranial nerve VI palsy is a common clinical presentation because of involvement of Dorello's canal (**Fig. 19**).[9,15,30–32] Nasopharyngeal cancer can also affect the parasagittal skull base through the foramen lacerum and by means of V3 perineural extension along the foramen ovale.[22]

JNA is a vascular neoplasm occurring exclusively in adolescent boys. It originates in the posterior nasal fossa in the region of the sphenopalatine foramen, extending into the pterygopalatine fossa and, from

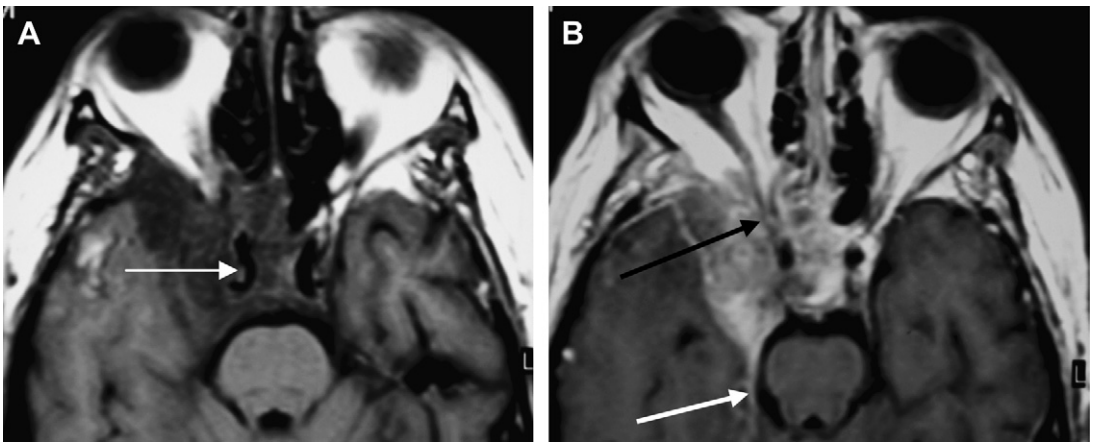

Fig. 17. Axial pregadolinium (*A*) and postgadolinium (*B*) T1-weighted images show a large sphenocavernous lesion on the right extending anteriorly into the orbital apex and sphenoethmoid sinuses, laterally into the middle cranial fossa and lateral wall of the orbit, and posteriorly along the right tentorial leaflet. The lesion encases the right cavernous carotid without narrowing its lumen (*white arrow in A*) and replaces the body of the sphenoid, clivus, and greater sphenoid wing. Postcontrast enhancement is slightly heterogeneous, and a dural tail is noted along the tentorium (*white arrow in B*). Note the encasement and compression of the optic nerve at the optic canal (*black arrow in B*) and secondary proptosis (intradiploic sphenocavernous meningioma).

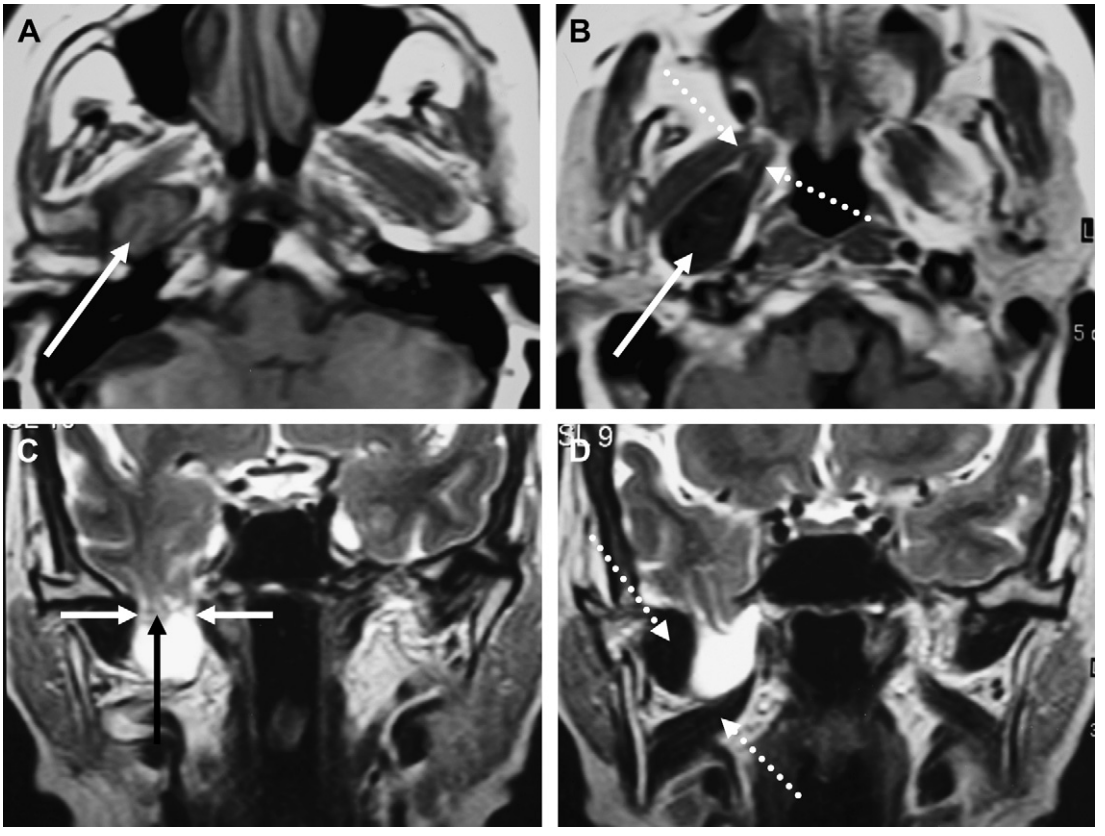

Fig. 18. Axial T1W (*A and B*) show a mixed lesion with solid (*white arrow in A*) and cystic (*white arrow in B*) components on the right parasagittal central skull base centred on foramen ovale and extending into the masticator space in between the medial and lateral pterygoid muscles (*dashed white arrows in B and D*). Coronal T2W images (*C and D*) clearly demonstrate a bony defect at the greater sphenoid wing involving the region of foramen ovale (*white arrows*) with herniation of the intracranial contents, both meninges and the inferior temporal gyrus (*black arrow*), into the masticator space (basal transphenoidal meningoencephalocele).

there, into the parasagittal skull base by way of the foramen rotundum or the vidian canal.[3,4,9,11,12] These highly vascular tumors demonstrate intense contrast enhancement in an early arterial phase and may show a "salt and pepper" pattern on MR imaging, with the salt corresponding to the tumor stroma or hemorrhage and the pepper corresponding to vascular flow voids (**Fig. 20**).[9,11,12] Recurrent epistaxis is the rule. Clinical setting, location, and imaging features are pathognomonic.

Lateral Central Skull Base Lesions

The lateral CSB includes the far lateral aspect of the greater sphenoid wings, the lateral aspect of the temporal bone, and the TMJ. On axial imaging, the anterior-lateral aspect of the greater sphenoid wing has a grossly triangular shape, usually referred to as the sphenoid triangle (**Fig. 21**A white arrows). This anatomic region constitutes a crossroad between the orbit, the middle cranial fossa, and the temporal fossa (suprazygomatic masticator space) and can be affected by any lesion originating from these compartments.[3,4,8]

Globular, and particularly intradiploic (en plaque), meningiomas are of common occurrence in this region, seen on CT as extensive bone sclerosis, often with an irregular contour mimicking osteoblastic metastases or osteosarcoma.[9,11–15] On MR imaging, they show low signal intensity

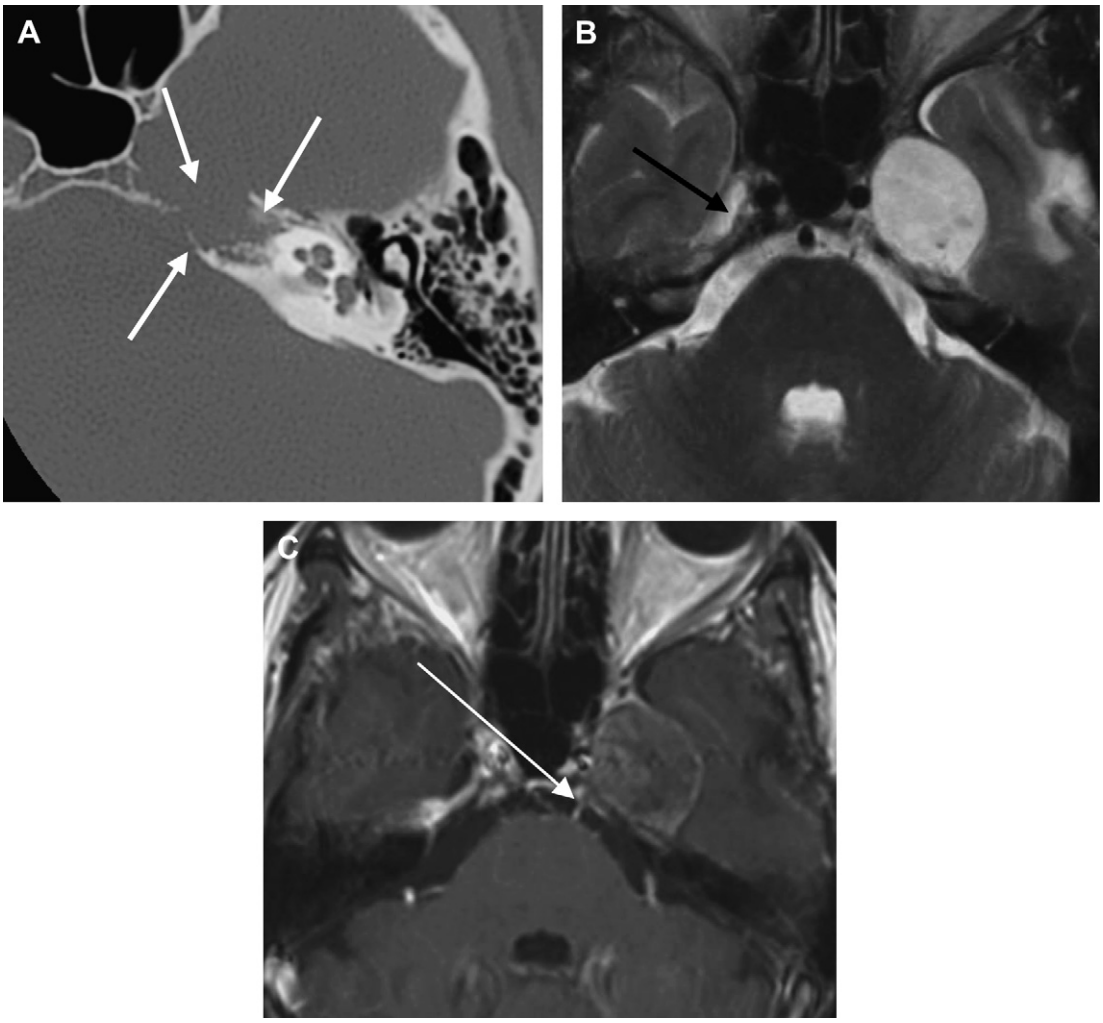

Fig. 19. (*A*) Axial CT scan in a high-resolution bone algorithm shows a lytic destructive lesion on the left petroclival region (*white arrows*). (*B*) Axial T2-weighted and (*C*) postgadolinium axial T1-weighted images show an expansile lesion in the left petroclival region. The lesion is of high signal intensity on T2-weighted images, similar to CSF, and shows only slight to moderate enhancement after administration of gadolinium. It involves cranial nerve IV (*white arrow in C*) at Dorello's canal and obliterates Meckel's cave (note the normal cave on the contralateral side; *black arrow in B*). No gross calcifications are noted within the lesion (petroclival chondrosarcoma).

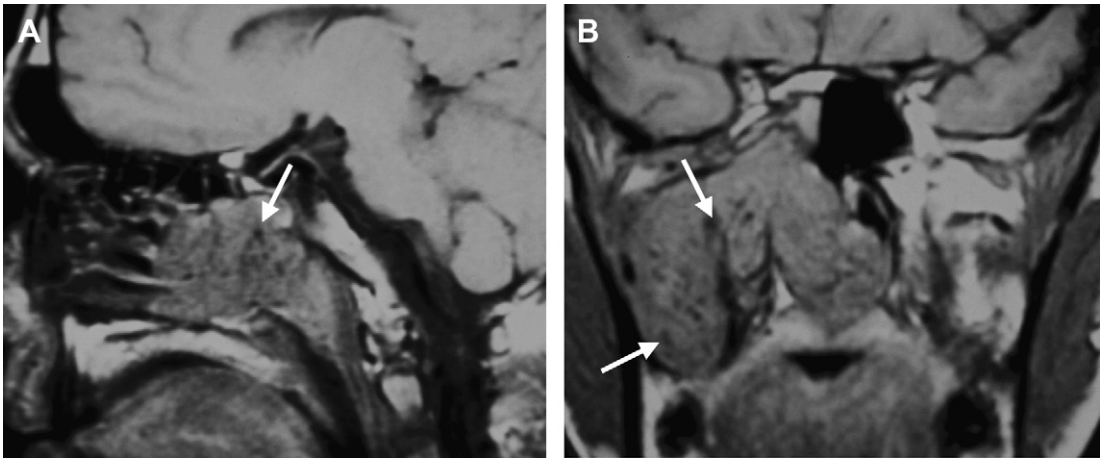

Fig. 20. Axial (*A*) and coronal (*B*) T1-weighted MR images show a large lesion centered in the right pterygopalatine fossa, extending laterally into the masticator space through the pterygomaxillary fissure, medially into the posterior nasal cavity through the sphenopalatine foramen, and posteriorly and superiorly along the vidian canal and foramen rotundum. The lesion is slightly lobulated in contour but is well marginated. Also, note the presence of serpentine flow voids (*white arrows*) reflecting its hypervascular nature (JNA).

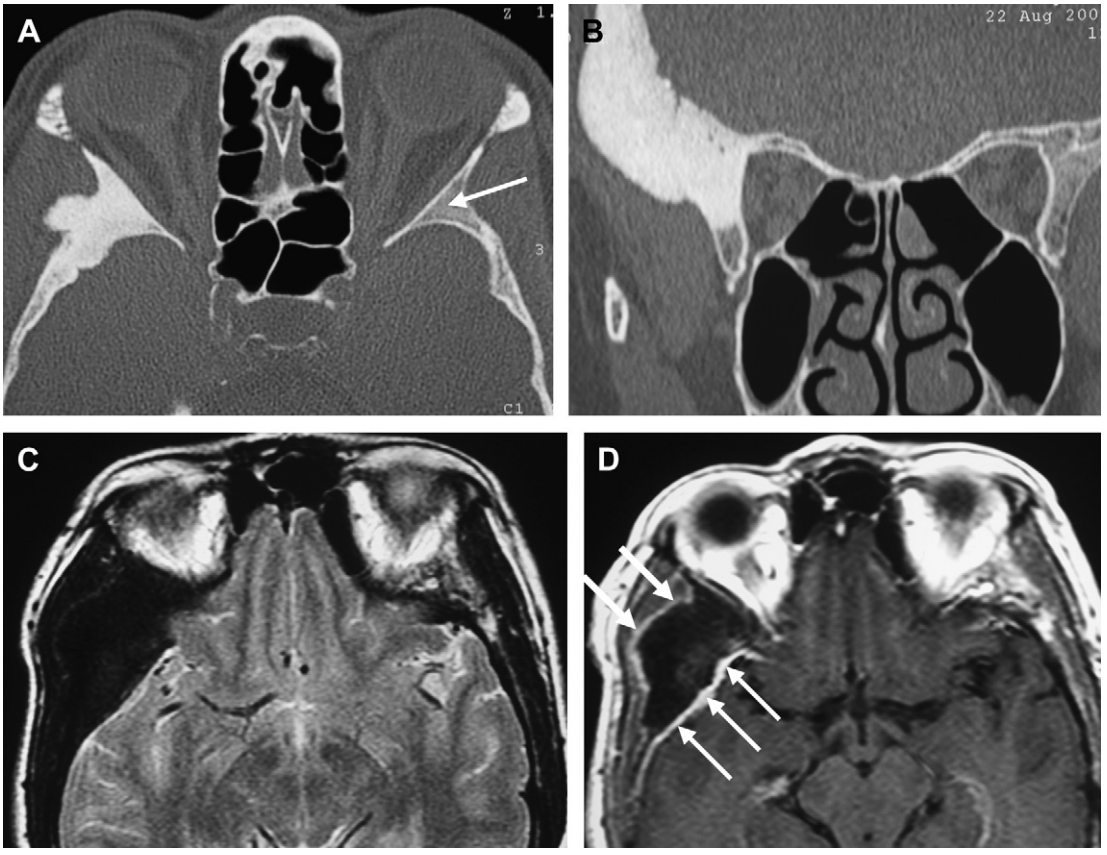

Fig. 21. (*A, B*) Axial and coronal CT images in a bone algorithm demonstrate an expansile sclerotic lesion in the lateral CSB involving the sphenoid triangle and lateral orbital wall, bulging medially into the middle cranial fossa and laterally into the suprazygomatic masticator space (note the sphenoid triangle on the normal side- *white arrow*). On the axial T2-weighted image (*C*), the lesion follows the signal intensity of compact bone (signal void), and on the postgadolinium axial T1-weighted image (*D*), it shows only peripheral enhancement (*white arrows*) (intradiploic meningioma).

on T1- and T2-weighted images and on gadolinium enhancement, with a dural tail along the middle cranial fossa (see **Fig. 21**).[9,15]

Lesions arising from the TMJ are site specific and include a variety of tumors and tumor-like conditions and infectious-inflammatory processes that may spread into the middle cranial fossa. Synovial chondromatosis and benign and malignant synovial tumors can all arise in this synovial joint.[9,33,34]

Pigmented villonodular synovitis can occasionally extend into the middle cranial fossa along the greater sphenoid wing. The hallmark of this lesion is the presence of frond-like hyperplastic synovium; blood degradation products attributable to repeated hemorrhage; and giant foam cells containing hemosiderin, which are responsible for the heterogeneous signal intensity on MR imaging and relative hyperdensity on plain CT studies.[9,33,34] Frond-like enhancement is the rule.[9,33,34] Pressure erosion on the articular surfaces leads to expansion of the joint space and remodeling of adjacent bone.[9,33,34]

Chondroblastoma or chondromatous giant cell tumor is an exclusively epiphyseal neoplasm that is exceedingly rare in the skull base. It may occasionally originate in the mandibular condyle, affect the TMJ, and grow into the lateral CSB.[35,36] Around 90% of cases are diagnosed before the age of 30 years. On CT, it presents as an expansile, eccentric, lytic lesion with geographic margins and a lobulated contour. Calcifications, punctate or irregularly shaped, are seen in approximately half of the cases, and joint involvement, often with effusion, may occur.[35,36] MR imaging tends to overestimate tumor aggressiveness. The tumor matrix is of intermediate to low signal intensity on T1- and T2-weighted images, except when associated with an aneurysmal bone cyst (highly hyperintense on T2-weighted images, often with fluid-fluid levels).[35,36] Peripheral enhancement is the rule (**Fig. 22**).

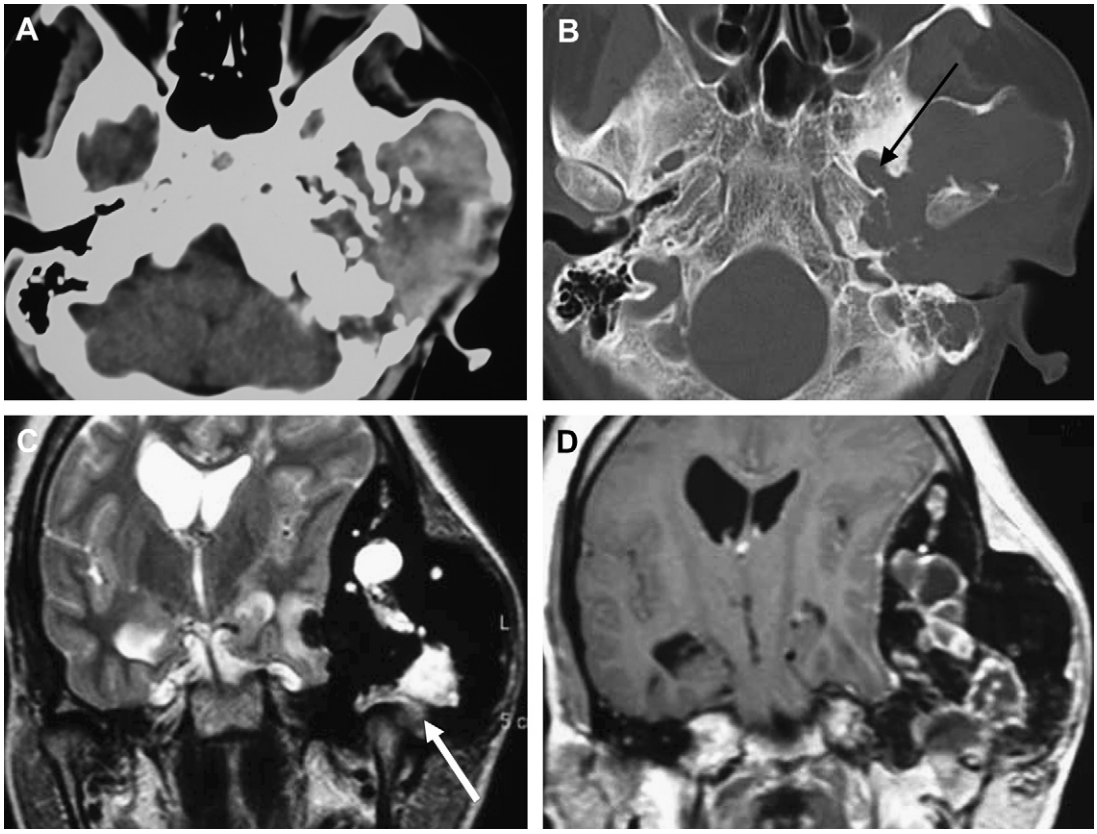

Fig. 22. Axial CT images in soft tissue (*A*) and a bone window (*B*) show a large lytic lesion expanding the lateral aspect of the greater sphenoid wing, temporal bone, and glenoid cavity and involving the left TMJ. Extensive bone remodeling and thinning, with some areas of bony dehiscence and fine bony septa, are also shown. Note the bony dehiscence on the lateral margin of the foramen ovale (*black arrow*). Coronal T2-weighted (*C*) and postgadolinium T1-weighted (*D*) images show to advantage the craniocaudad extent of the lesion, the presence of multiple cysts, and joint effusion (*white arrow in C*). Also, note the dramatic mass effect upon the intracranial structures (chondroblastoma).

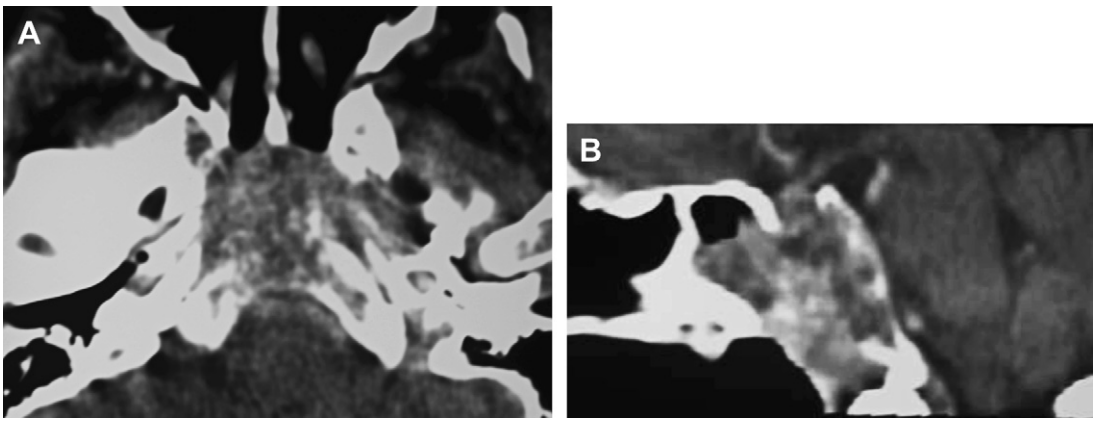

Fig. 23. Contrast-enhanced axial (*A*) and sagittal (*B*) CT reconstruction on a soft tissue window show a destructive lytic lesion centered on the clivus and eroding its cortical margins, with an associated soft tissue mass enhancing heterogeneously in a man with a prior history of colonic adenocarcinoma (clival metastasis).

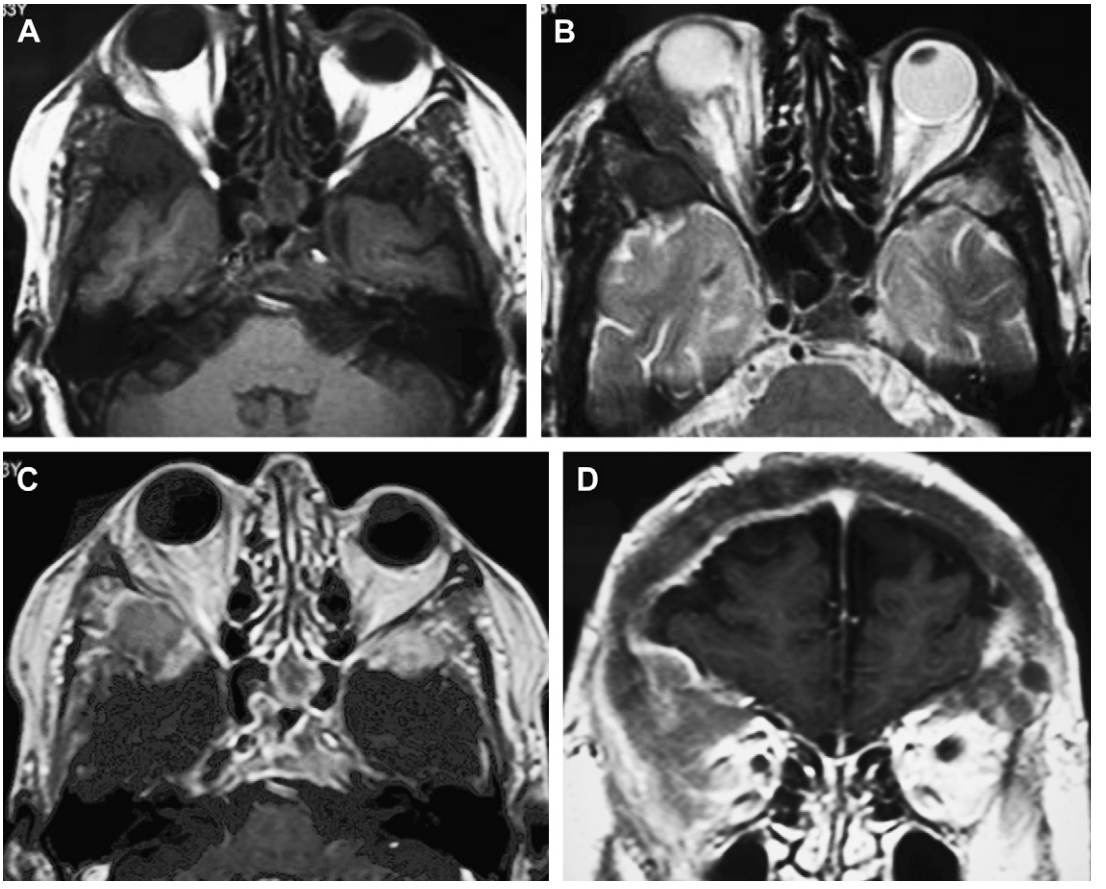

Fig. 24. Axial T1-weighted image (*A*), T2-weighted image (*B*), and contrast-enhanced axial (*C*) and coronal (*D*) T1-weighted images show multiple predominantly sclerotic lesions (hypointense on T1-weighted and T2-weighted images) in the lateral aspect of the greater sphenoid wing, sphenoid triangle, and lateral orbital wall, which enhance vividly on the postgadolinium images. Except for the enhancement, the imaging features are similar to those shown in Fig. 21 (bone metastases from prostate cancer).

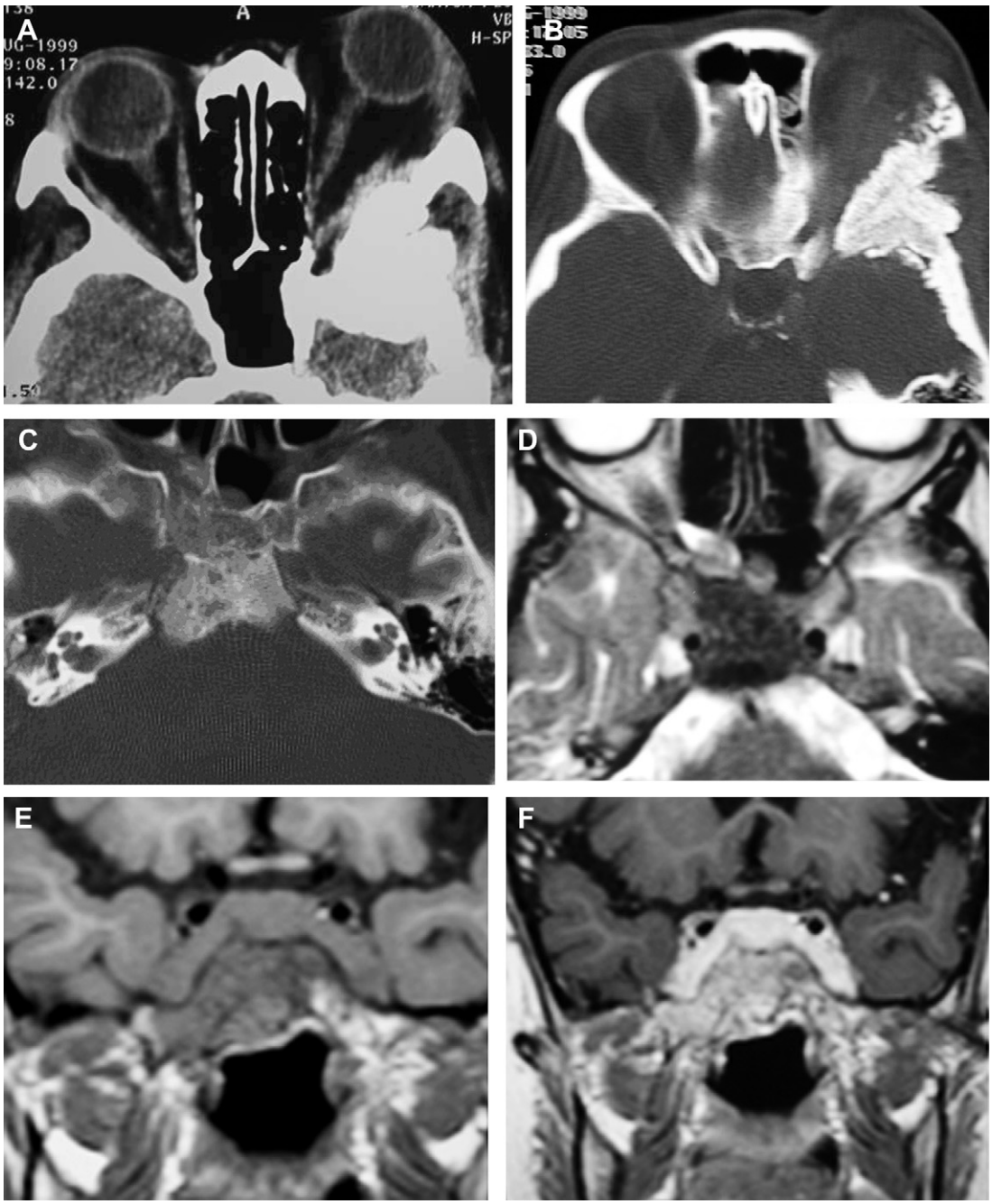

Fig. 25. Axial CT images on soft tissue (*A*) and in a bone window (*B*) show an expansile sclerotic lesion in the left sphenoid triangle and lateral orbital wall with an aggressive sunburst pattern of periosteal reaction leading to proptosis (osteogenic osteosarcoma). (*C*) Axial CT image in a bone window in another patient shows a permeative lesion involving the clivus that is predominantly sclerotic but has small ill-defined lytic areas. Axial T2-weighted image (*D*) and coronal precontrast (*E*) and postcontrast (*F*) T1-weighted images in the same patient show that the lesion is markedly hypointense on T2-weighted imaging, is of intermediate signal intensity on T1-weighted imaging, and enhances vividly after gadolinium administration. The lesion bulges inferiorly in the left nasopharyngeal roof (osteosarcoma secondary to prior irradiation of a posterior fossa medulloblastoma).

Intrinsic Non–Site-Specific Central Skull Base Lesions

Primary and secondary bone neoplasms, fibro-osseous conditions, a variety of systemic bone diseases, and infection can occur in any of the subdivisions of the CSB.

Metastasis is the most common neoplasm affecting the skull base in an adult patient; therefore, it should be included in the differential diagnosis of any intrinsic skull base lesion.[3,4,9,11–15] Because bone metastases are mostly attributable to hematogenous spread, they tend to occur in bones with higher marrow content, such as the clivus, petrous apex, sphenoid triangle, and diploe of the calvarium.[9,11–15] Lesions are primarily centered in the bony structures of the skull base and can be lytic, sclerotic, or mixed (**Figs. 23** and **24**). The lung, breast, prostate, and kidney are the most common primaries to metastasize to the skull base.[4,9,12] Occasionally, a skull base metastasis can be the presenting feature of a neoplasm elsewhere, although malignant disease is already known in most cases. Osteoblastic metastasis can mimic an intradiploic meningioma or an osteosarcoma.[9,14,15] When diffuse, bone metastases can be mistaken for Paget's disease or other fibro-osseous conditions (**Fig. 24**). Hypervascular metastases, such as those from the kidney, thyroid, melanoma, carcinoid, or choriocarcinoma, can potentially be confused with other hypervascular lesions, such as paragangliomas, JNAs, hemangiopericytomas, and meningiomas.[9,11,12]

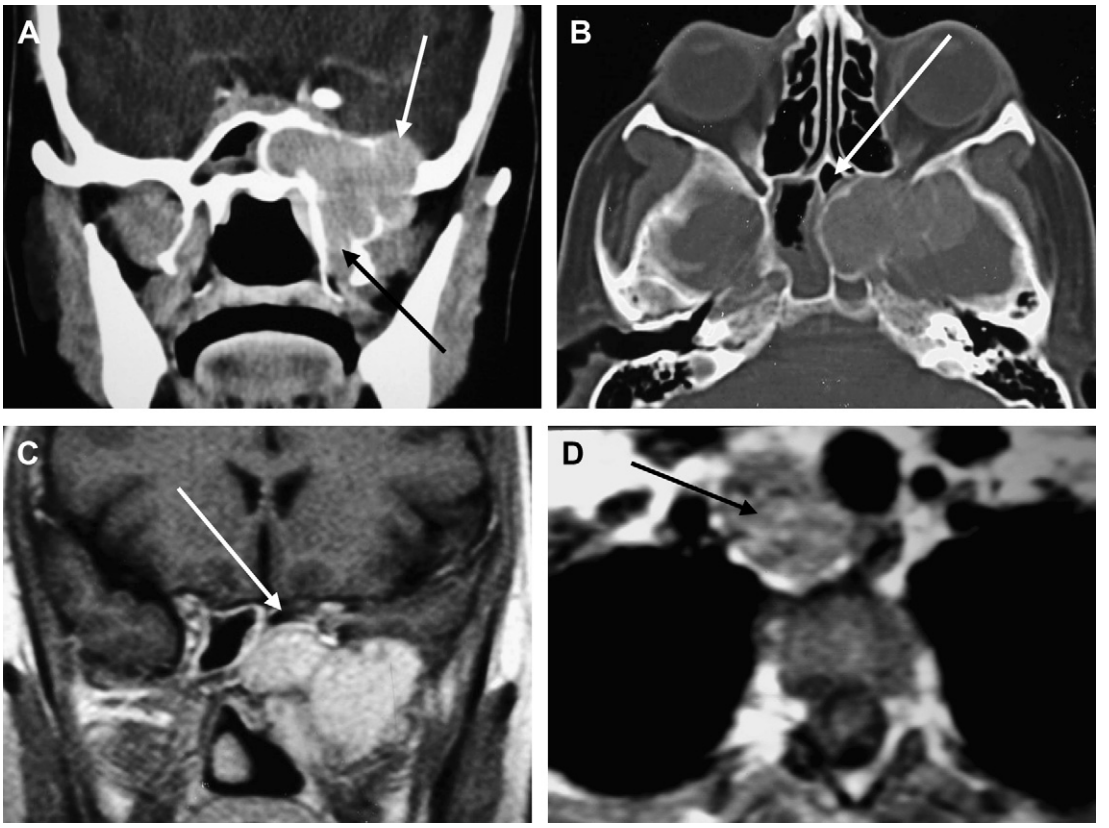

Fig. 26. Contrast-enhanced coronal CT image on soft tissue (*A*), axial CT image on a bone algorithm (*B*), and coronal postgadolinium MR imaging (*C*) demonstrate a well-defined expansile lesion centered in the greater sphenoid wing, bulging medially into the sphenoid sinus (partially obliterated by the lesion) (*white arrows in B and C*), bulging superiorly into the middle cranial fossa (*white arrow in A*), and bulging inferiorly into the pterygoid plates (*black arrow in A*). Note the bone remodeling and thinning without frank bone erosion, suggesting a slow-growing benign process. Also note the vivid enhancement of the lesion. (*D*) Axial T1-weighted image through the lower neck shows a rounded mass lesion on the right tracheoesophageal groove immediately below the inferior pole of the right thyroid lobe (*black arrow in D*) (brown tumor attributable to primary hyperparathyroidism).

Plasmacytoma and multiple myeloma can occur in the skull base, presenting as an expansile destructive lytic lesion with a soft tissue component spontaneously hyperdense on CT scans and showing intermediate signal intensity on T1- and T2-weighted MR imaging.[9,14,15] These imaging features are typical for hypercellular, small, round-cell tumors with a high nucleo-cytoplasmic ratio, which is also a hallmark of lymphoma and leukemic infiltrates (chloromas/granulocytic sarcomas).

In the skull base the most common primary malignant bone tumor is osteosarcoma. This are of rare occurrence in the skull base, often secondary to prior radiation therapy or Paget's disease. Osteosarcomas are characterized by new bone formation and by an aggressive pattern of periosteal reaction, with a spiculated hair-on-end or sunburst appearance, which is best depicted on CT scans (**Fig. 25**).[9,12,14,15]

Any benign bone tumor can potentially occur in the skull base and share the same imaging features as elsewhere. Giant cell tumors, such as osteoclastoma, aneurysmal bone cyst, and brown tumor, are remarkable for the presence of multinucleated giant cells and hemosiderin-laden macrophages secondary to intratumoral hemorrhage and may not be differentiated from each other on the basis of pathologic findings alone.[9,37] The presence of iron, in the form of hemosiderin and ferritin, accounts for tumor hyperdensity on plain CT scans and low signal intensity on T2-weighted MR imaging, with a blooming effect on T2* sequences attributable to susceptibility artifact.[37] These are usually benign-appearing, slow-growing, expansile lytic lesions that remodel and thin cortical bone (**Fig. 26**).[9,37] The diagnosis of brown tumors is supported by laboratory findings of hyperparathyroidism.[9,37] These are highly vascularized

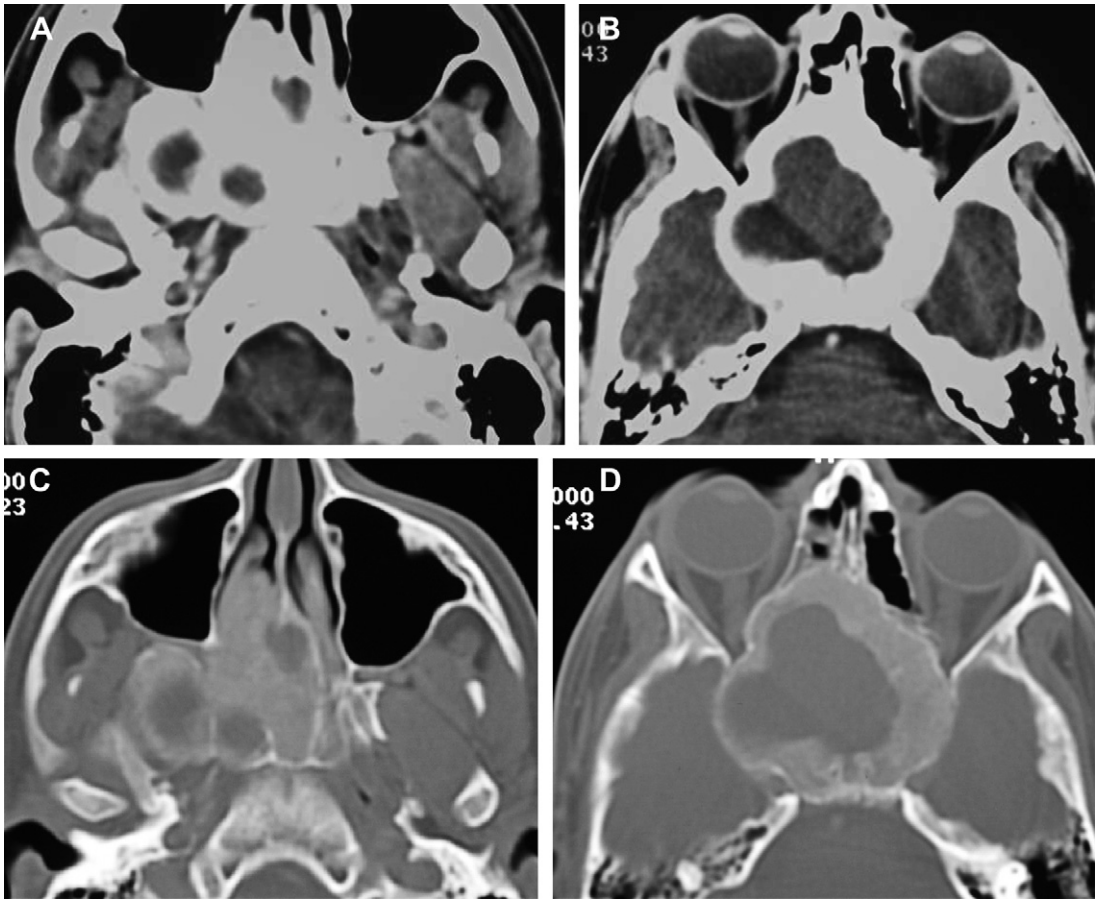

Fig. 27. Axial CT images on soft tissue (*A* and *B*) and bone window (*C* and *D*), show an expansile lesion centered in the sphenoid body, which obliterates the sphenoid sinus extends inferiorly into the pterygoid plates and anteriorly into the posterior nasal septum and nasal turbinates. The lesion is homogeneously hypodense, surrounded by a thick rim of sclerotic bone with a ground-glass pattern excluding sphenoid mucocele as a possible diagnosis (ossifying fibroma).

lesions demonstrating vivid enhancement after contrast administration.[9,37]

Osteoblastoma can seldom be seen in the skull base. It is a benign bone-forming neoplasm of children and young adults, usually presenting before the age of 30 years.[3,4,9] Imaging shows a sharply circumscribed, expansile, predominantly lytic or mixed lytic-sclerotic lesion depending on the degree of mineralization of the tumor matrix, often in the form of bony septa.[9,15] A peripheral sclerotic rim resembling an eggshell is the rule.

Fibro-osseous conditions, such as fibrous dysplasia, ossifying fibroma, and Paget's disease, can affect the skull base. Overall, CT is more specific in the diagnosis, although MR imaging can provide additional information regarding disease activity.

Fibrous dysplasia is primarily a disease of the medullary cavity, sparing cortical bone, which is an important distinctive feature from Paget's disease.[3,4,9,38,39] Woven bone is replaced by myxofibrous tissue with different degrees of mineralization depending on the phase of disease activity. Initially, cystic spaces, more or less coalescent, predominate; a mixed-sclerotic pattern with a ground-glass appearance then ensues; and, finally, intense mineralization results in a sclerotic pattern.[9,38,39] Bone expansion is the rule, which may lead to stenosis of skull base neurovascular foramina and to secondary neurologic deficits.[9,38,39] Affected bones tend to merge imperceptibly with normal-appearing bones.[38,39] A periosteal reaction, when present, indicates pathologic fracture or malignant degeneration, most often into osteosarcoma.[9,14,15,38,39] Contrast-enhanced MR imaging can be used to determine whether the disease is active (showing moderate to intense enhancement) or quiescent (non-enhancing).[15,38,39]

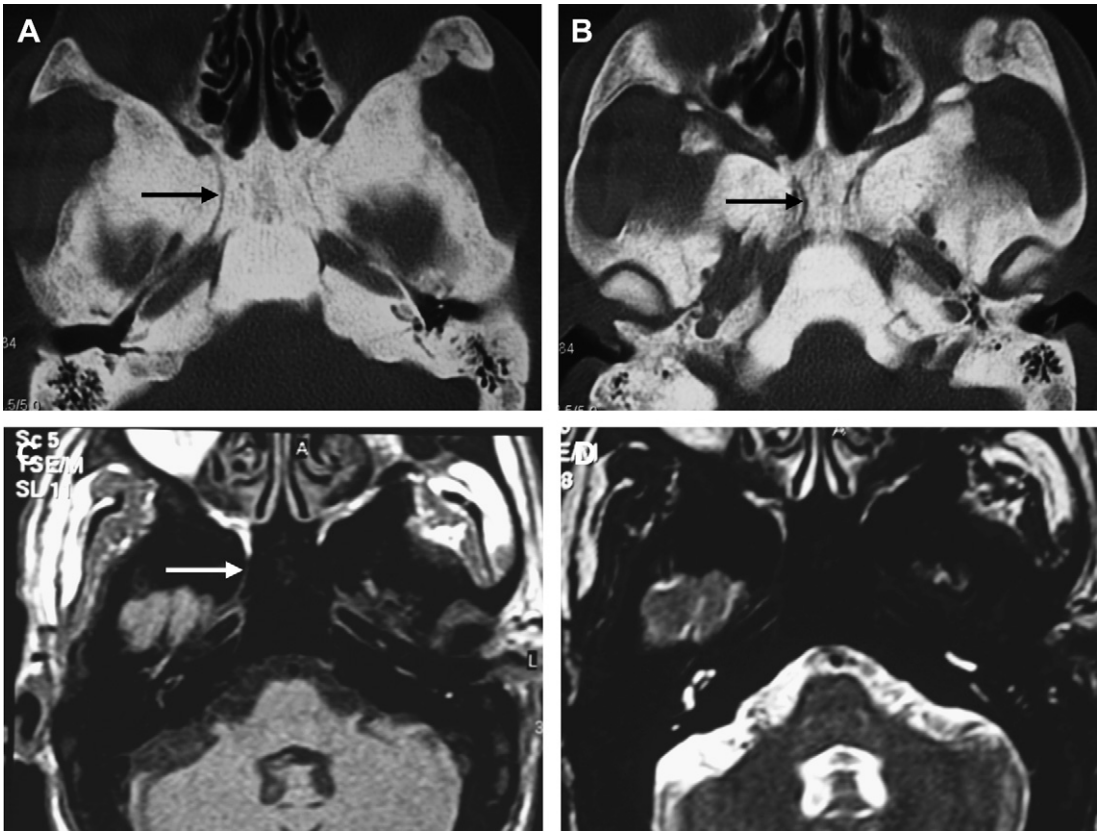

Fig. 28. (*A*, *B*) Axial CT images on a bone algorithm show diffuse skull base osteosclerosis with obliteration of the normal trabecular pattern by dense, amorphous, and structureless bone. Note the involvement of the temporal bone including the otic capsule. Axial T1-weighted (*C*) and T2-weighted (*D*) images show extensive signal void of the entire skull base reflecting the replacement of the bone marrow by dense compact bone. There is slight bone expansion leading to stenosis of the neurovascular foramina of the skull base. Note the stenotic foramen rotundum compressing V2 (*black arrows in A and C*) and the vidian canal (*white arrow in B*).

Ossifying fibroma is a monostotic form of fibrous dysplasia with a more aggressive behavior. It often leads to marked bone expansion and compressive signs and symptoms (**Fig. 27**).[9,38,39]

Whereas fibrous dysplasia is a disease of children and young adults, Paget's disease tends to occur beyond the fifth decade of life. It thickens cortical bone, and although lytic, mixed, and sclerotic stages are also recognized, the hallmark of the disease is bone expansion and sclerosis with coarse bony trabecula. As opposed to fibrous dysplasia, it may affect the otic capsule.[3,4,9,38,39]

Osteopetrosis is a rare hereditary disorder, leading to defective osteoclast function and loss of normal bone resorption and remodelling.[4] Bones become thick and sclerotic with an increased propensity to fracture. Bone expansion in the skull base may lead to compressive neurovascular symptoms and signs (**Fig. 28**).[4,9,11,12]

Eosinophilic granuloma is part of the spectrum of Langerhans' cell histiocytosis, a pathologic condition characterized by the presence of a histiocytic-like cell. It is seen in the pediatric age group and manifests as a punched-out lytic lesion without marginal sclerosis and with bevelled edges.[9,11,12] Spontaneous hyperdensity on CT and intermediate to low signal intensity on T2-weighted MR imaging are the rule, imposing the differential diagnosis with other small round-cell tumors (**Fig. 29**).[9,11]

Skull base osteomyelitis can result from the spread of infection, usually from the sinonasal region or middle ear cavity, often caused by aggressive bacterial or invasive fungal infections in immunocompromised hosts.[9,12] Invasive forms of *Aspergillus* and *Mucor* species and *Pseudomonas aeruginosa* infections in the form of malignant or necrotizing otitis externa are most commonly seen. Invasive funguses are remarkable for their angiocentric growth, leading to vessel irregularity, stenosis, and occlusion.[9,12,14,15] On

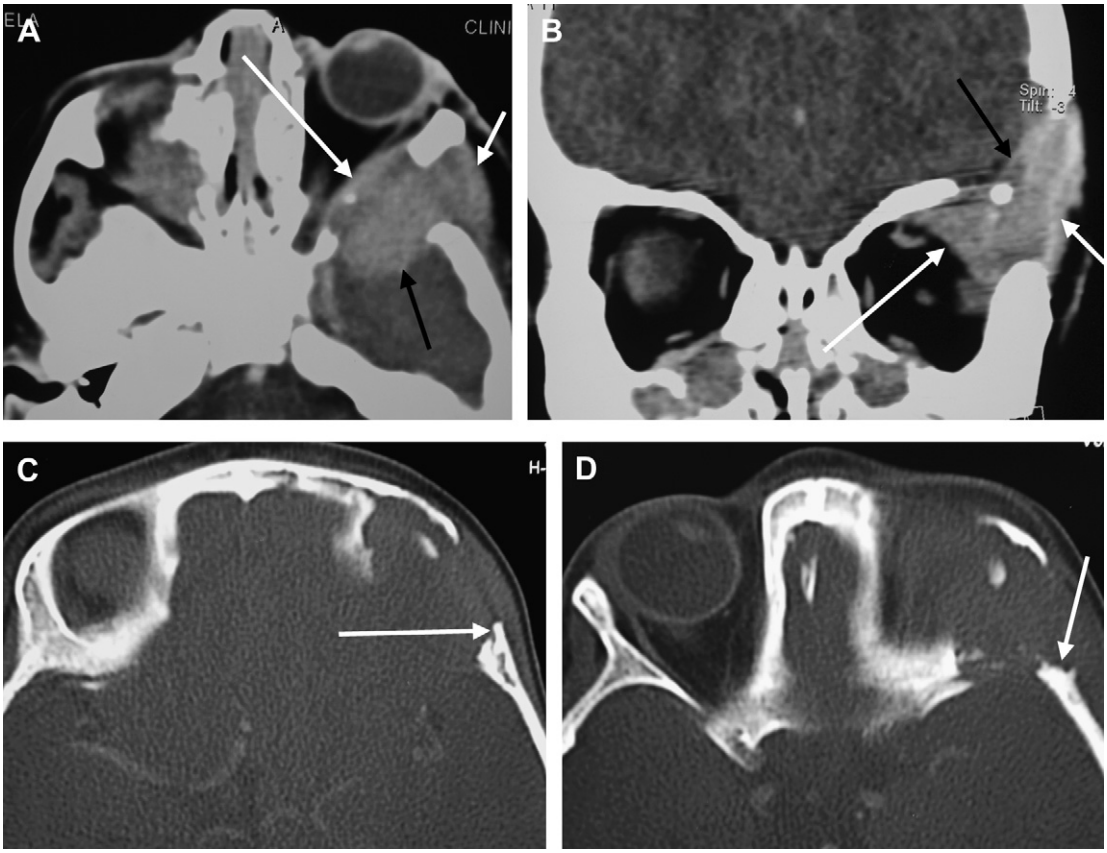

Fig. 29. Contrast-enhanced axial (*A*) and coronal (*B*) CT images in soft tissue window show a vividly enhancing mass lesion on the left sphenoid triangle bulging medially into the orbit (*long white arrows*), laterally into the suprazygomatic masticator space (*short white arrows*) and posteriorly into the middle cranial fossa (*black arrows*). Axial images on a bone algorithm (*C and D*) show a lytic expansile lesion with bevelled edges (*white arrows*) in a 9 month old child (Langerhans cell histyocitosis).

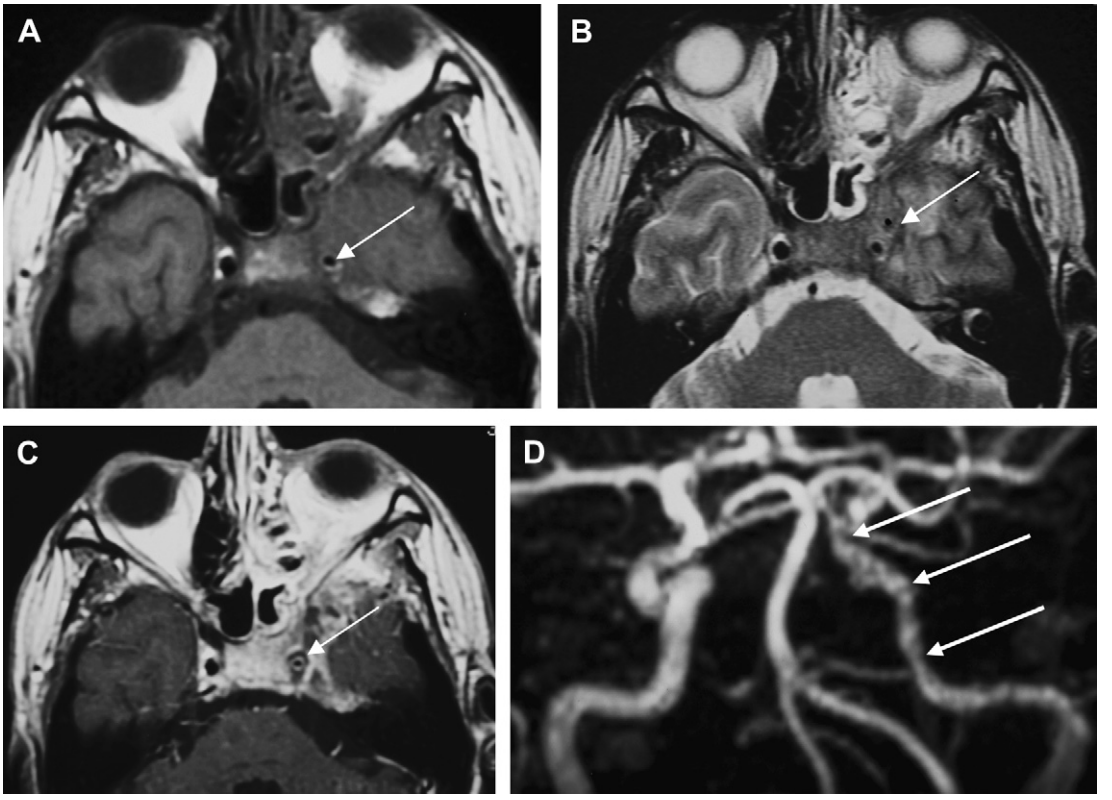

Fig. 30. Axial T1-weighted (*A*), T2-weighted (*B*), and postgadolinium T1-weighted (*C*) images show extensive replacement of the central bony skull base by a soft tissue mass that extends from the nasal cavity and paranasal sinuses into the pterygopalatine fossa and inferior orbital fissure and, posteriorly, into the left cavernous sinus encasing the left internal carotid artery (*white arrows in A–C*). This soft tissue mass is of low signal intensity on the T2-weighted images and enhances intensely after administration of gadolinium. Magnetic resonance angiography, (*D*) demonstrates to advantage the stenosis and irregularity of the lumen of the left internal carotid artery along the petrous and cavernous segments (*white arrows*).

imaging, the presence of extensive bone and cartilaginous destruction in excess of the amount of associated soft tissue in an adequate clinical setting suggests the diagnosis (**Fig. 30**).[9,12] Brain infarcts are a possible complication when the intracranial vessels is involved.[11,12,15]

Necrotizing otitis externa begins as an infection of the external auditory canal and may secondarily spread to the parotid space inferiorly, medially into the tympanic cavity, and, from there, anteriorly into the petrous apex and clivus and posteriorly into the jugular foramen. Internal jugular vein and dural sinus thromboses are common complications of this aggressive infection.[9,22]

SUMMARY

Cross-sectional imaging has a pivotal role in the evaluation of the CSB, which has limited clinical access. Lesions affecting this anatomic area may arise primarily from the skull base proper or from neurovascular structures traveling through the skull base or may arise secondarily from lesions originating from the intracranial compartment or from the extracranial head and neck. Subdivision of the CSB into middle, off-midline, and lateral compartments and knowledge of the anatomic structures contained in each of these compartments are useful in limiting differential diagnoses. Putting together the clinical setting, location, and cross-sectional imaging features and playing with the statistics can provide a good approximation of the final diagnosis. Additionally, and most importantly, imaging is used to provide the exact mapping of the CSB and to plan surgical or focused radiation therapy with increasing accuracy.

ACKNOWLEDGMENTS

The author acknowledges Drs. David Coutinho, Fernando Torrinha, Sérgio Cardoso, Domingos Coiteiro, Robert Lufkin, Bert de Foer, and Jan Casselman for providing her with some of the

images presented in this article and thanks the departments of ENT, Head and Neck Surgery, and Pathology of the Cancer Institute of Lisbon for their continuing support.

REFERENCES

1. Durden DD, Williams DW III. Radiology of skull base neoplasms. Otolaryngol Clin North Am 2001;34(6): 1043–64.
2. Som PM, Curtin HD. Head and neck imaging, skull base. 4th edition. St. Louis (MO): Mosby Year Book; 2003. p. 261–373, 783–863.
3. Curtin HD, Chavali R. Imaging the skull base. Radiol Clin North Am 1998;36(5):801–17.
4. Atlas SW. Magnetic resonance imaging of the brain and spine. 3rd edition. Philadelphia: Lippincott Williams & Wilkins; 2002.
5. Weber AL. Imaging of the skull base. Eur J Radiol 1996;22(1):68–81.
6. Pierot L, Boulin A, Guillaume A, et al. Imaging of skull base tumours in adults. J Radiol 2002;83: 1719–34.
7. Ehab Y, Hanna, DeMonte Franco. Comprehensive management of skull base tumours. 1st edition. New York, London: Informa healthcare; 2009.
8. Borges A. Skull base tumours part I: imaging technique, anatomy and anterior skull base tumours. Eur J Radiol 2008;66:338–47.
9. Borges A. Skull base tumours part II: central skull base tumours and intrinsic tumours of the bony skull base. Eur J Radiol 2008;66:348–62.
10. Chong VF, Fan YF, Tng CH. Pictorial review: radiology of the sphenoid bone. Clin Radiol 1998;53: 882–93.
11. Fishbein NJ, Kaplan MJ. Magnetic resonance imaging of the central skull base. Top Magn Reson Imaging 1999;10(5):325–46.
12. Casselman JW. The skull base: tumoral lesions. Eur Radiol 2005;15(3):534–42.
13. Borges A, Casselman J. Imaging the cranial nerves: part I: methodology, infection and inflammatory, traumatic and congenital lesions. Eur Radiol 2007; 17(8):2112–25.
14. Lufkin R, Borges A, Villablanca P. Teaching atlas of head and neck imaging. 1st edition. New York: Thieme; 2000. p. 3–31, 82–104, 303–36, 370–80.
15. Lufkin R, Borges A, Nguyen K, et al. MRI of the head and neck. 2nd edition. MRI Teaching File Series. Philadelphia: Lippincott Williams & Wilkins; 2001.
16. Tomura N, Hirano H, Sashi R, et al. Comparison of MR imaging and CT in discriminating tumour infiltration of cortex and bone marrow in the skull base. Comput Med Imaging Graph 1998;22(1):41–51.
17. Borges A, Lufkin R, Huang A, et al. Frequency-selective fat-suppression MR imaging: localized asymmetric failure of fat suppression mimicking orbital disease. J Neuroophthalmol 1997;17(1): 12–7.
18. Casselman J, Mermuys K, Delanote J, et al. MRI of the cranial nerves—more than meets the eye: technical considerations and advanced anatomy. Neuroimaging Clin N Am 2008;18(2):197–231.
19. Ishida H, Mohri M, Amatsu M. Invasion of the skull base by carcinomas: histopathologically evidenced findings with CT and MRI. Eur Arch Otorhinolaryngol 2002;259(10):535–9.
20. Patel SG, Singh B, Polluri A, et al. Craniofacial surgery for malignant skull base tumours: report of an international collaborative study. Cancer 2003; 98(6):1179–87.
21. Clayman GL, DeMonte F, Jaffe DM, et al. Outcome and complications of extended cranial-base resection requiring microvascular free-tissue transfer. Arch Otolaryngol Head Neck Surg 1995;121(11): 1253–7.
22. Chong FH, Khoo BK, Fan YF. Imaging of the nasopharynx and skull base. Magn Reson Imaging Clin N Am 2002;10:547–71.
23. Pamir MN, Ozduman K. Analysis of radiological features relative to histopathology in 42 skull base chordomas and chondrosarcomas. Eur J Radiol 2006;58(3):461–70.
24. Crockard A. Chordomas and chondrosarcomas of the cranial base: results and follow-up of 60 patients. Neurosurgery 1996;38(2):420–7.
25. Yu Q, Wang P, Shi H, et al. Central skull base invasion of maxillofacial tumours: computed tomography appearance. Oral Surg Oral Med Oral Pathol Oral Radiol Endod 2000;89(5):643–50.
26. Borges A, Casselman J. Imaging the cranial nerves: part II: primary and secondary neoplastic conditions and neurovascular conflicts. Eur Radiol 2007;17(9): 2332–44.
27. Majoie CB, Hulsmans FJ, Castelijns JA, et al. Primary nerve sheath tumours of the trigeminal nerve: clinical and MR findings. Neuroradiology 1999;41:100–8.
28. Borges A. Trigeminal neuralgia and facial nerve palsy. Eur Radiol 2005;15(3):511–33.
29. Williams LS. Advanced concepts in the imaging of perineural spread of tumour to the trigeminal nerve. Top Magn Reson Imaging 1999;10:376–83.
30. Neff B, Sataloff RT, Storey L, et al. Chondrosarcoma of the skull base. Laryngoscope 2002;112(1): 134–9.
31. Rosenberg AE, Nielsen GP, Keel SB, et al. Chondrosarcoma of the skull: a clinicopathologic study of 200 cases with emphasis on its distinction from chordoma. Am J Pathol 1999;23:1370–8.

32. Rosenberg AE, Brown GA, Bhan AK, et al. Chondroid chordoma—a variant of chordoma. A morphologic and immunohistochemical study. Am J Pathol 1994;101:36–41.
33. Chow LT, Kumta SM, King WW. Extra-articular pigmented villonodular synovitis of the temporomandibular joint. J Laryngol Otol 1998;112(2):182–5.
34. Tanaga K, Suzuki M, Nameki H, et al. Pigmented villonodular synovitis of the temporomandibular joint. Arch Otolaryngol Head Neck Surg 1997;123(5): 536–9.
35. Bui P, Ivan D, Olivier D, et al. Chondroblastoma of the temporomandibular joint: report of a case and literature review. J Oral Maxillofac Surg 2009;67(2):405–9.
36. Gaudet EL Jr, Nuss DW, Johnson DH Jr, et al. Chondroblastoma of the temporal bone involving the temporomandibular joint, mandibular condyle and middle cranial fossa: case report and review of the literature. Cranio 2004;22(2):160–8.
37. Connor SE, Umaria N, Chavda SV. Imaging of giant tumours involving the anterior skull base. Br J Radiol 2001;74:662–7.
38. Slootweg PJ. Maxillofacial fibro-osseous lesions: classification and differential diagnosis. Semin Diagn Pathol 1996;13:104–12.
39. Chong VF, Khoo JB, Fan YF. Fibrous dysplasia involving the base of the skull. AJR Am J Roentgenol 2002;178:717–20.